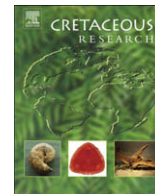


Contents lists available at [ScienceDirect](http://www.sciencedirect.com)

## Cretaceous Research

journal homepage: [www.elsevier.com/locate/CretRes](http://www.elsevier.com/locate/CretRes)

## Organic carbon deposition and phosphorus accumulation during Oceanic Anoxic Event 2 in Tarfaya, Morocco

Haydon P. Mort<sup>a,\*</sup>, Thierry Adatte<sup>a,2</sup>, Gerta Keller<sup>b</sup>, David Bartels<sup>b</sup>, Karl B. Föllmi<sup>a,2</sup>, Philipp Steinmann<sup>a,2</sup>, Zsolt Berner<sup>c</sup>, E.H. Chellai<sup>d</sup>

<sup>a</sup>Rue Emile Argand 11, Institute of Geology, University of Neuchâtel, Case postale 158, CH-2009 Neuchâtel, Switzerland

<sup>b</sup>Department of Geosciences, Princeton University, Guyot Hall, Princeton, NJ 08544-1003, USA

<sup>c</sup>Institut für Mineralogie und Geochemie, Universität Karlsruhe, 76128 Karlsruhe, Germany

<sup>d</sup>University Cadi Ayyad, Faculty of Sciences Semailia, Marrakech, Morocco

## ARTICLE INFO

## Article history:

Received 23 September 2006

Accepted in revised form 4 May 2008

Available online xxx

## Keywords:

Anoxia

Phosphorus burial

Organic carbon

Morocco

Cenomanian-Turonian

## ABSTRACT

With a multi-proxy approach, an attempt was made to constrain productivity and bottom-water redox conditions and their effects on the phosphorus accumulation rate at the Mohammed Plage section on the Tarfaya coast, Morocco, during the Cenomanian–Turonian Anoxic Event (OAE 2). A distinct  $\delta^{13}\text{C}_{\text{org}}$  isotope excursion of +2.5‰ occurs close to the top of the section. The unusually abrupt shift of the isotope excursion and disappearance of several planktonic foraminiferal species (e.g. *Rotalipora cushmani* and *Rotalipora greenhornensis*) in this level suggests a hiatus of between 40–60 kyrs at the excursion onset. Nevertheless, it was possible to determine both the long-term environmental history as well as the processes that took place immediately prior to and during OAE 2. TOC% values increase gradually from the base of the section to the top (from ~2.5% to ~10%). This is interpreted as the consequence of a long-term eustatic sea-level rise and subsidence causing the encroachment of less oxic waters into the Tarfaya Basin. Similarly a reduction in the mineralogically constructed ‘detrital index’ can be explained by the decrease in the continental flux of terrigenous material due to a relative sea-level rise. A speciation of phosphorus in the upper part of the section, which spans the start and mid-stages of OAE 2, shows overall higher abundances of  $P_{\text{reactive}}$  mass accumulation rates before the isotope excursion onset and lower values during the plateau. Due to the probable short hiatus, the onset of the decrease in phosphorus content relative to the isotope excursion is uncertain, although the excursion plateau already contains lower concentrations. The  $C_{\text{org}}/P_{\text{total}}$  and  $V/\text{Al}$  ratios suggest that this reduction was mostly likely caused by a decrease in the available bottom oxygen content (probably as a result of higher productivity) and a corresponding fall in the phosphorus retention ability of the sediment. Productivity appears to have remained high during the isotope plateau possibly due to a combination of ocean-surface fertilisation via increased aridity (increased  $K/\text{Al}$  and  $\text{Ti}/\text{Al}$  ratios) and/or higher dissolved inorganic phosphorus content in the water column as a result of the decrease in sediment P retention. The evidence for decreased P-burial has been observed in many other palaeoenvironments during OAE 2. Tarfaya’s unique upwelling paleosituation provides strong evidence that the nutrient recycling was a global phenomenon and therefore a critical factor in starting and sustaining OAE 2.

© 2008 Elsevier Ltd. All rights reserved.

### 1. Introduction

At least seven so-called ‘anoxic events’ punctuated various intervals in the Cretaceous of which one occurred in the latest Cenomanian (Bonarelli Level) dated around 93.5 Ma. Generally these events are characterized by enhanced organic-rich shale deposition

and positive  $\delta^{13}\text{C}$  excursions (Schlanger and Jenkyns, 1976; Jenkyns, 1980). Although the fundamental causal mechanisms have remained enigmatic, there have been no shortages of ideas that have, at least in part, helped to explain these events. The causal nature of each OAE is likely to be subtly different given the differing sea-level positions, tectonic and paleogeographic situations (Haq et al., 1987; Jenkyns, 1991; Hallam and Wignall, 1999; Aguilera-Franco et al., 2001) and ocean chemistry at each point in time. In terms of the amount and rate of organic carbon sequestration OAE 2 was probably the largest of the anoxic events that punctuated the Cretaceous. Often the debate has centred on the role of preservation and productivity in producing the characteristic positive  $\delta^{13}\text{C}$

\* Corresponding author.

E-mail address: [h.mort@geo.uu.nl](mailto:h.mort@geo.uu.nl) (H.P. Mort).

<sup>1</sup> Present address: Department of Earth Sciences - Geochemistry, Faculty of Geosciences, Utrecht University, PO Box 80.021, 3508 CD Utrecht, The Netherlands.

<sup>2</sup> Present address: Institut de Géologie et de Paléontologie, IGP, Université de Lausanne, Anthropôle, CH-1015 Lausanne, Switzerland.

excursion and black shales. Ideas revolving around increased anoxia and the expansion of the oxygen minimum zone (OMZ) find universal agreement (e.g., [Sinninghe Damsté and Koster, 1998](#); [Keller et al., 2001](#)) when explaining black shale formation. However disagreement remains as to the driving force of the increased anoxic conditions; whether it is productivity driven (i.e. organic rich sediments were formed only through the rate at which organic matter was arriving at the sea-floor) (e.g. [Kuypers et al., 2002](#)), or preservation where productivity itself would not have been enough to sustain black-shale deposition. Bacterial respiration of organic matter and the resulting decrease in oxygen availability inhibited the breakdown of organic matter ([Sinton and Duncan, 1997](#); [Racki and Cordey, 2000](#); [Mort et al., 2007a](#)).

Increased continental nutrient run-off triggered by elevated CO<sub>2</sub> driven temperatures, evaporation, precipitation and weathering have been the most commonly cited mechanism to explain increased productivity (e.g. [Larson and Erba, 1999](#)). This model fails to reconcile conflicting clay mineral data obtained from OAE 2 sequences, which suggest increased aridity rather than chemical weathering ([Jeans et al., 1991](#); [Sellwood et al., 1994](#)). The sea-level transgression, leading up to OAE 2, probably played a significant role, potentially decreasing the erosional capacity of rivers due to higher base levels, flood and leaching nutrients on previous dry land and causing the encroachment of waters with low oxygen availability higher onto the shelf. Clearly there are great uncertainties and inconsistencies in our knowledge as to how the ocean/atmosphere system has led to the repeated occurrence of OAEs during the Cretaceous.

## 2. Geological and tectonic setting

Mohammed Plage is a coastal section located at the northern end of the Tarfaya Basin, Morocco. The Tarfaya Basin extends along the southern coast of Morocco between 28°N and 24°N. The basin is situated at the tectonically stable western margin of the Saharan Platform ([Fig. 1A and 1B](#)). The Mohammed Plage section is situated on the eastern flank of a wide synclinal structure. Throughout the region, during the late Cenomanian to early Turonian, laminated, organic-rich siltstones, limestones, and marls were deposited in an open shelf environment to depths of 200–300 m ([Kuhnt et al., 2001](#)). According to [Gebhardt et al. \(2004\)](#), the palaeoenvironment shallows to the north of the basin. Thus, at Mohammed Plage the depositional setting was likely interpreted as being near the paleo-coastline associated with high terrigenous input.

The similar subsidence history of the Western Pyrenean and Basque Basins shows how large an area was being affected by subsidence during the Late Cretaceous and how it probably played an important role in the long-term palaeoenvironmental shifts that took place in the region. A variety of proxies suggest a gradual subsidence began in the late Albian. ([Schwenke and Kuhnt, 1992](#)) used sedimentological and benthic foraminiferal data to construct decompacted and back-stripped subsidence histories, which probably varied in the several sub-basins along the axis of the Betic Seaway ([Reicherter et al., 1994](#)).

Eustatic sea-level rises inferred from the Russian Platform and Western Europe are in the order of 70 m during the Cenomanian ([Sahagian et al., 1996](#); [Gräfe, 2002](#)). Therefore out of the total reported 150 m of relative sea-level rise in the Tarfaya Basin, 80 m could be accounted for by subsidence alone ([El Albani et al., 1999a,b](#); [Gebhardt et al., 2004](#)).

This gradual subsidence appears to have been punctuated by at least 9 sea-level lowstands ([Gebhardt et al., 2004](#)), as indicated by the abundance of shallow water benthic foraminifera (tolerance range 20–100 m; *Bolivina anambra*, *Lenticulina spissocosta* and *Spiroplectammia* sp.). Despite these regressions, the migration of ostracod species indicates that a Trans-Saharan seaway may have existed flowing south to north especially during the late Cenomanian ([Gebhardt, 1999](#)).

## 3. Geochemistry and cyclostratigraphy

Modern (South China Sea) and ancient studies (on the Tarfaya coast) show that benthic foraminiferal assemblages are strongly modulated by carbon flux and oxygenation fluctuations ([Holbourn et al., 1999](#); [Kuhnt et al., 1999](#); [Holbourn and Kuhnt, 2002](#)). Given that the oxidation of organic matter is decelerated when the oxygen minimum zone impinges on the shelf sea during sea-level highstands, the gradual relative sea-level (RSL) rise (150 m) could explain the gradual increase in total organic carbon (TOC) contents throughout the Mohammed Plage section ([Kolonic et al., 2002](#); [Gebhardt et al., 2004](#)). [Kuhnt et al., 1997](#) noted that maximum organic carbon burial corresponds to benthos-free laminated sediments, which indicates bottom water anoxia.

In the same study, [Kuhnt et al. \(1997\)](#) constructed the first cyclostratigraphic framework for the Cenomanian-Turonian sediments in the region, by using density logs from six exploration wells. The attributed cyclic fluctuations in organic carbon and pelagic carbonate content were presumed to have arisen from climate changes driven by Cretaceous obliquity (39 ka) Milankovitch cycles. ([Kolonic et al., 2005](#)) reassessed the cyclicity to have been eccentricity. They made a well correlation to the Mohammed Plage section to calculate bulk sedimentation rates, which were then used to generate mass accumulated rates for TOC and redox sensitive metals. High amplitude variations in these proxies lead the authors to conclude that this geochemical response resulted from short-term fluctuations in the upwelling ([El Albani et al., 1999b](#)) of oxygen depleted, nutrient-rich intermediate waters coupled to enhanced marine productivity. Climate forcing supposedly drove photic zone and bottom water euxinia, alternating with periods of better water column oxygenation.

General circulation models (GCMs) also predict the location of a major upwelling zone on the North African margin during much of the Late Cretaceous ([Bush and Philander, 1997](#)). The presence of this zone made the Tarfaya Basin an extremely productive area of the ocean.

In this study, a variety of traditional and novel proxies is employed in order to more accurately reconstruct the late Cenomanian palaeoenvironmental history of the Tarfaya Basin. A better understanding of the environmental factors that lead to the development of OAE 2 may be generated by evaluating the behaviour of geochemical proxies prior to and during the  $\delta^{13}\text{C}$  excursion.

## 4. Material and methods

The Mohammed Plage section was measured and sampled at closely spaced intervals of 10 to 30 cm. For this study a total of 121 samples was analyzed, which span the mid-late Cenomanian including the critical OAE 2 interval that starts ~17 m above the base of the cliff ([Fig. 2](#)).

Foraminifera were prepared for biostratigraphic analysis using standard methods at the University of Princeton, N.J, U.S.A. (see [Keller et al., in press](#)). Because of the high organic content foraminifera were difficult to free from the indurated bituminous and slightly silicified chalk and therefore no quantitative analysis could be obtained. Thin sections were made for every second sample for biostratigraphic analyses. The resultant species ranges and relative abundance estimates are based on thin sections and washed residues.

Bulk rock and clay mineralogical analyses were carried out on a SCINTAG XRD 2000 diffractometer at the University of Neuchâtel, Switzerland, following the procedure outlined by ([Kübler, 1987](#); [Adatte et al., 1996](#)). Accuracy was better than 5%. Bulk rock contents were obtained using standard semiquantitative techniques based on external standardization. XRD analysis was also made on the <2  $\mu\text{m}$  sediment fraction to determine the abundance of major clay mineral components.

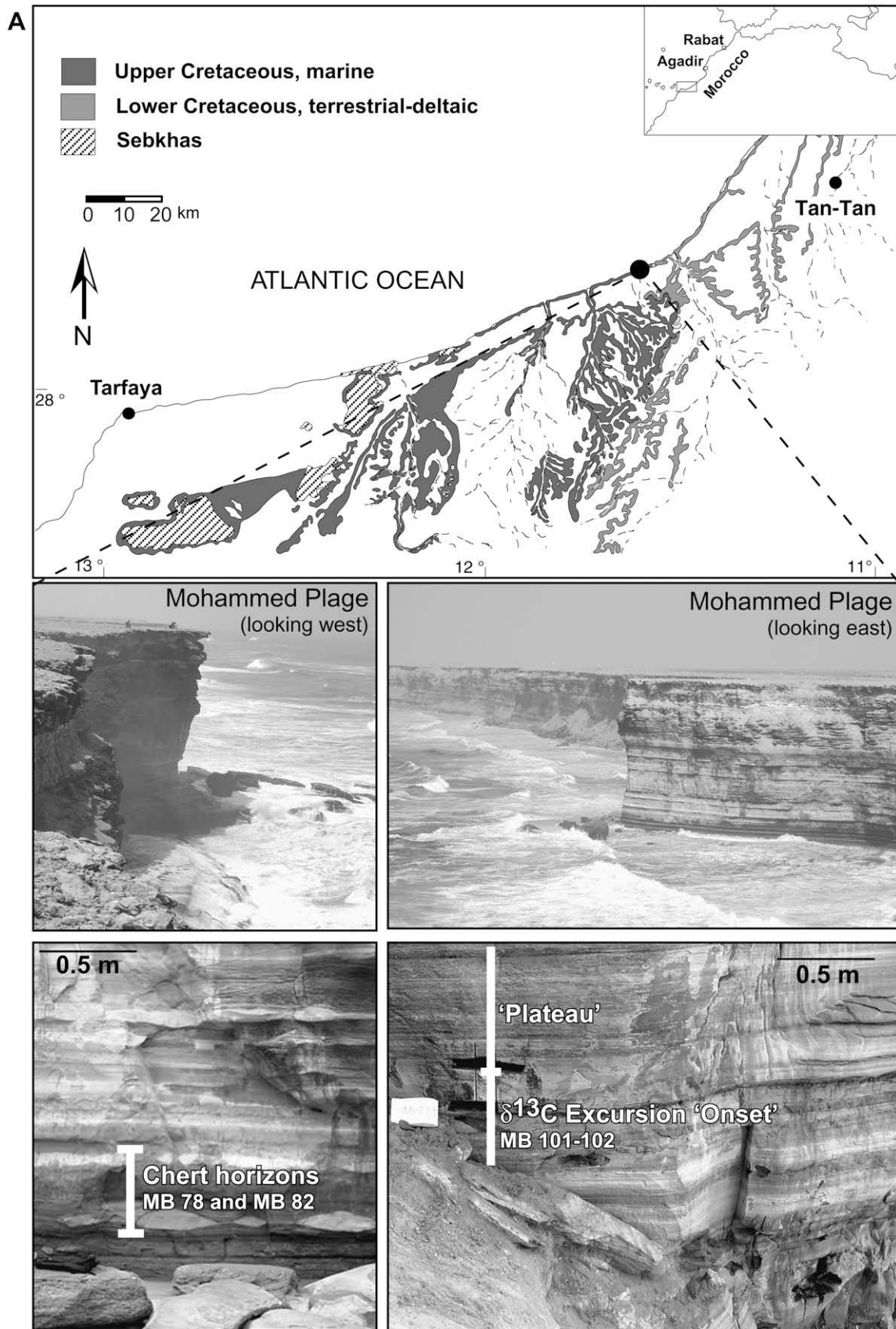


**Fig. 1.** A, Position of the Mohammed Plage section on the modern coastline. Adapted from Gebhardt et al. (2004). Outcrop photographs show different perspectives of the section along with lithological details of the  $\delta^{13}\text{C}_{(\text{org})}$  excursion and chert nodule layer. B, Palaeogeographical map detailing the main depositional environments of the Peri-Tethyan realm, including North Africa in the late Cenomanian (94.7–93.5 Ma). Modified after (Philip, 2003). The Mohammed Plage section is indicated. Also shown are the section of Eastbourne, Manilva and Furlo to which comparisons are made in the discussion.

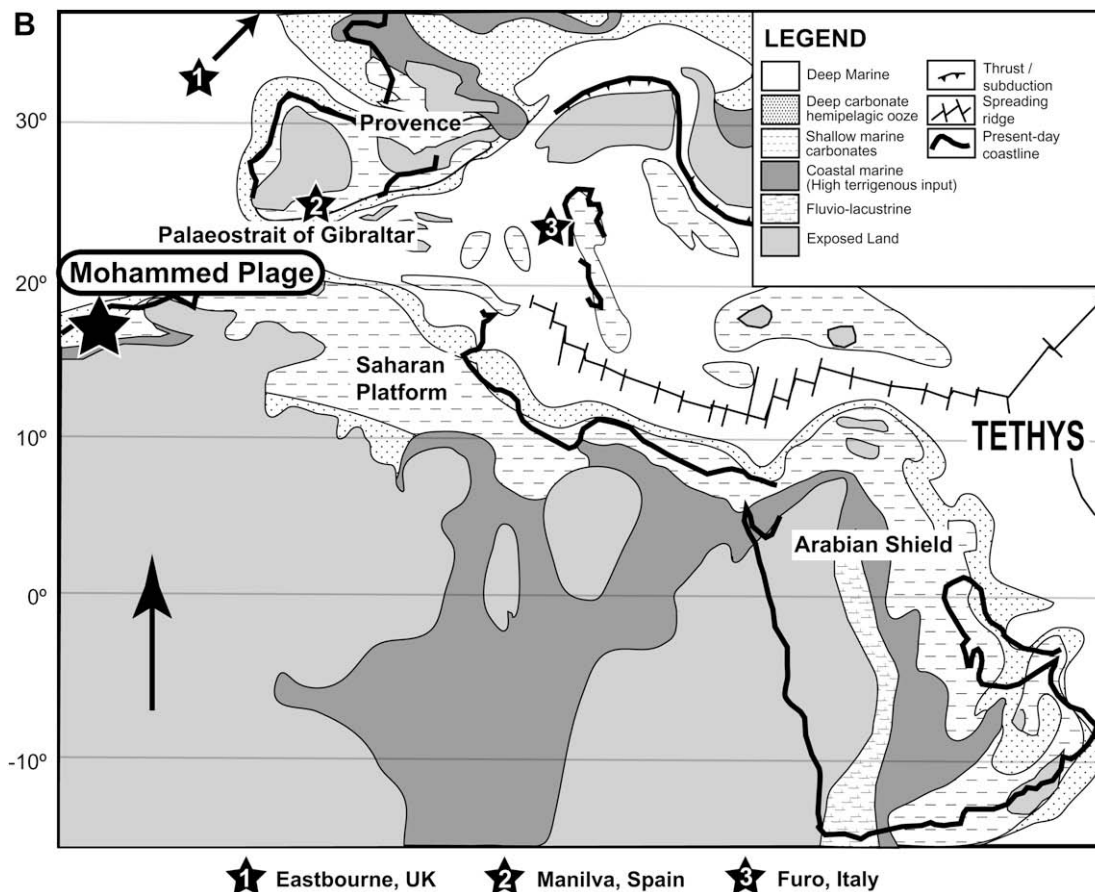


Fig. 1 (continued).

A detrital index (DI) was obtained by dividing the sum of quartz, feldspar, plagioclase and phyllosilicates intensities by calcite. Lower DI values therefore correspond to less delivery of terrigenous material from continental sources and/or increased dilution due to a greater marine influence.

The abundance of the different phosphorus phases was quantified following the sequential extraction (SEDEX) procedure (Ruttenberg, 1992; Eijsink et al., 1997; Anderson and Delaney, 2000). This method has been successfully applied to a wide range of geological and modern settings (Eijsink et al., 1997; Anderson and Delaney, 2000; Tamburini et al., 2003a; Tamburini et al., 2003b). Measurements for  $P_{\text{authigenic}}$ ,  $P_{\text{detrital}}$  and  $P_{\text{organic}}$  were conducted with a UV/Vis Perkin Elmer Lambda 10 spectrophotometer at the University of Neuchâtel. Error margins are < 5%.  $P_{\text{total}}$  was calculated by the addition of the measured concentrations (mg/g) of the phases derived from the SEDEX method.

Published sedimentation rates based on cyclostratigraphy were used for the Mohammed Plage section (Kuhnt et al., 1997; Kolonic et al., 2005). These sedimentation rates served to calculate mass accumulation rates for phosphorus by multiplying [P] mg/g by the sedimentation rate (cm/ka) and rock density (Attewell and Farmer, 1976).

100–200 mg of powder were exposed to two hydrochloric (HCl) and hydrofluoric (HF) acid washes to leach silicate and non-silicate elements respectively. The residue was left to dry in a sunbath. 5 ml of hot 1 M HCl was added to the sediments and allowed to cool. The solutions was transferred to a 25 ml volumetric flask and analyzed with a Perkin Elmer Instruments Optima 4300 DV Inductively Coupled Plasma-Optical Emission Spectrometer (ICP-OES) at the University of Princeton, NJ, USA.

The quantity of barium that is not associated with the aluminosilicate fraction ( $Ba^*$ ) was calculated using the method outlined by (Thompson and Schmitz, 1997).  $Ba^*$  is assumed to be derived from the formation of biogenic barite through the following calculation.

$$Ba_{(\text{normalised})} = Ba/Al_2O_3(\text{sample}) \times Al_2O_3(\text{average crust})$$

$$Ba^* = Ba_{(\text{normalised})} - Ba_{(\text{aluminosilicate})}$$

Analysis of organic carbon abundance and type was conducted on all samples using Rock-Eval 6™ with instrumental precision of < 2% (see (Espitalié et al., 1985) for details).

## 5. Results

### 5.1. Lithology

The Mohammed Plage section predominantly consists of alternating limestones, marly limestones and shales. There are frequently siltstones, especially towards the base of the section. Limestone units often show erosive lower contacts, which mark tempestite accumulation at many horizons. Bioturbation is common, particularly within limestone units, below 12 m.

The sediments attributed to the upper Cenomanian at Mohammed Plage consists of dark to light, organic-rich marls and limestones with chert nodules in some lower beds. This study focuses on OAE 2, the beginning of which can be taken as the start of the isotope excursion (MB 100). Samples 74–121 (17–24 m) cover pre-OAE and a considerable part of the excursion plateau. A 10 cm thick, organic-rich

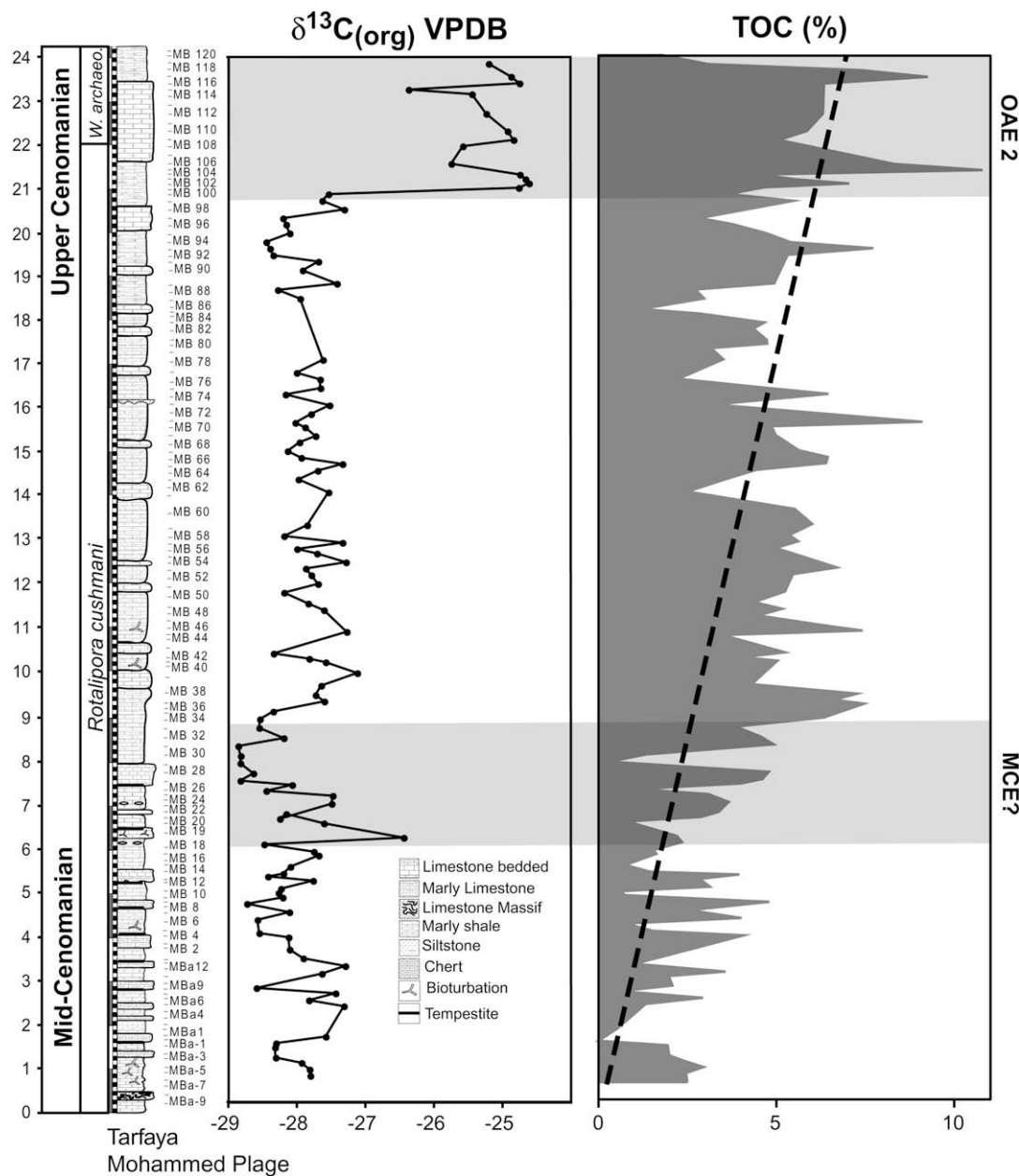


**Fig. 2.** Lithology with major sedimentary features and sample distribution plotted alongside  $\delta^{13}\text{C}_{(\text{org})}$  and TOC %. Note the gradual increase in TOC% values from the base-top of the section and the +2.5‰  $\delta^{13}\text{C}_{(\text{org})}$  excursion at 21 m.

limestone layer embedded with chert nodules defines the base of this interval. At the top of this layer is an erosional surface, followed by a 65 cm thick marly shale. A 20 cm thick, bedded marly limestone overlies this. This pattern of rhythmically bedded marly limestone and black shale repeats with few exceptions.

This lithologic sequence is similar to published lithologies of the Tarfaya Basin (e.g. Kuhnt et al., 2001; Gebhardt et al., 2004), suggesting that the Mohammed Plage section was deposited in a paleo-shelf environment. The erosive contacts between beds and the alternation between siltstone and limestone are indicative of sea level fluctuation.

## 5.2. Biostratigraphy

### 5.2.1. *Rotalipora reicheli* zone

At the Mohammed Plage section sediments attributed to the Cenomanian planktic foraminiferal zones *Rotalipora reicheli*, *R. cushmani* and *Whiteinella archaeocretacea* (Fig. 3) were studied. The *R.*

*reicheli* zone spans the range of the nominate taxon and the top coincides with the first appearance of *R. cushmani*. Two  $\delta^{13}\text{C}$  excursions mark this biozone in the Mohammed Plage section. The nannofossil biozone boundary CC9c/CC10a coincides with the top of the first excursion (sample MBa12) and the first appearance of *R. cushmani* is observed in the trough above the second excursion (sample MB30, Fig. 3). These two  $\delta^{13}\text{C}$  excursions appear to be the two mid-Cenomanian anoxic events (MCE 1 and 2), which Rodriguez et al. (1998) identified within the *R. reicheli* zone based on the Leioa section of the Basque basin in Spain. However, Coccioni and Galeotti (2003) placed the MCE events in the lower part of the *R. cushmani* zone based on the Bottaccione Gorge and Contessa quarry sections in Italy. The reason for the discrepancy in the zonal assignment is unclear at this time.

### 5.2.2. *Rotalipora cushmani* zone

The top of the *R. cushmani* zone is defined by the extinction of the nominate taxon. In the Tarfaya basin subsurface cores and Tazra

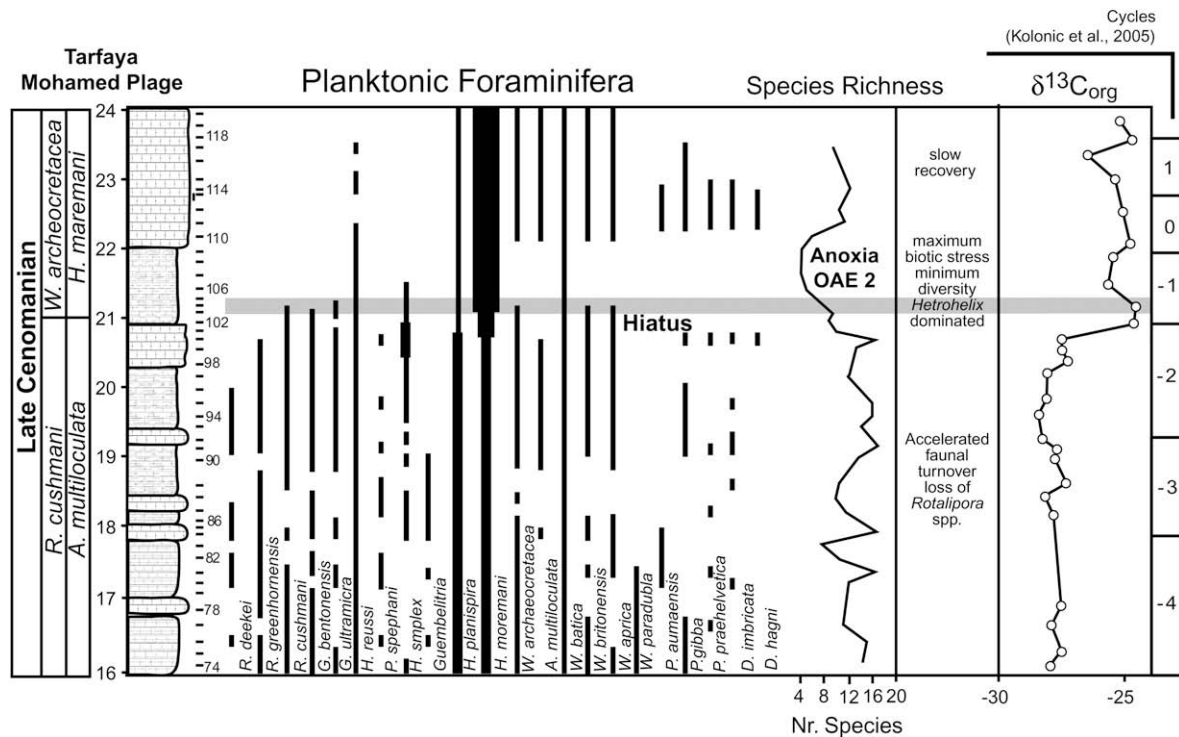


**Fig. 3.** Planktonic foraminiferal biostratigraphy showing the faunal changes before and during OAE 2 at Mohammed Plage. Note that the sharp faunal change coincident with the rapid  $\delta^{13}\text{C}_{\text{org}}$  shift and the lithological change marks a short hiatus that probably spans most of the onset of the excursion. However, the disappearance of *R. cushmani* at this level is likely an artifact of poor preservation and rarity of this species at the end of its range.

outcrop this extinction was observed after the  $\delta^{13}\text{C}$  shift that characterizes OAE 2, and more precisely in the trough between the first and second  $\delta^{13}\text{C}$  peaks about 70–90 cm above the maximum  $\delta^{13}\text{C}_{\text{carb}}$  excursion (Luderer and Kuhnt, 1997). At Mohammed Plage the last *R. cushmani* was observed 60 cm above the maximum excursion (sample MB103) and just below the trough. The absence of *R. cushmani* in the trough in our samples is likely due to poor preservation and the rarity of this species at the end of its range. *Rotalipora greenhornensis* disappears at the abrupt shift in  $\delta^{13}\text{C}_{\text{org}}$ , coincident with the onset of dominant low oxygen tolerant biserial species (*Heterohelix moremani* and *H. reussi*) and a lithological change from limestone to dark shale (Fig. 3). This suggests the presence of a short hiatus.

### 5.2.3. *Whiteinella archeocretacea* zone

This biozone spans the interval from the *Rotalipora cushmani* extinction to the first appearance of *Helvetoglobotruncana helvetica*, which marks the Cenomanian/Turonian (C/T) boundary. The uppermost part of the Mohammed Plage section does not reach the C/T boundary. The *Whiteinella archeocretacea* Zone is characterized by high abundance of *Heterohelix*, low species diversity and anoxic to dysoxic conditions. At Mohammed Plage the shift to dominant low oxygen tolerant *heterohelicids* (~60%, sample 101) begins at the top of a limestone layer and is coincident with the  $\delta^{13}\text{C}_{\text{org}}$  shift. A further increase to ~80% begins near the base (sample 103, Fig. 3) of the overlying dark shale. This shift to low oxygen tolerant *Heterohelix* dominated assemblages is globally recognized and marks the onset of the *H. moremani* subzone (Keller and Pardo, 2004). The lower part of this subzone is characterized by minimum diversity and maximum biotic stress. The upper part sees the return of *Whiteinella*, *Dicarinella* and *Praeglobotruncana*.

### 5.3. Stable carbon isotopes (organic carbon)

For the majority of the Mohammed Plage section  $\delta^{13}\text{C}$  values remain low, fluctuating between  $-28.5\text{‰}$  and  $-27.5\text{‰}$  (see Fig. 2),

except for two exceptions. The first shift represents the mid-Cenomanian Event (MCE), which consists of a small peak in  $\delta^{13}\text{C}$  values ( $-26.4\text{‰}$ ) in sample MB 18, followed by a trough ( $-28.82\text{‰}$ ) in samples MB 26–30 (total shift  $-2.42\text{‰}$ ). The second shift represents the OAE 2 and consists of an abrupt  $+2.59\text{‰}$  shift in sample MB 97, ~21 m above the base of the section. This shift, marked by four initial points, represent the first of two  $\delta^{13}\text{C}$  peaks separated by a trough, as documented in many previous studies (Gale et al., 1993; Paul et al., 1999; Keller et al., 2001; Tsikos et al., 2004). The following 'plateau' values show similar amplitude variations ( $\sim 1\text{‰}$ ) to those lower in the section. The abrupt nature of the OAE 2 isotope excursion suggests a significant hiatus between samples MB 100 and MB 101. A comparison with the  $\delta^{13}\text{C}_{\text{org}}$  and  $\delta^{13}\text{C}_{\text{carb}}$  curves of nearby subsurface cores S13, S57 and S75 (Kuhnt et al., 2005; Tsikos et al., 2004; Kolonic et al., 2005) provides an approximate duration for the hiatus. In Mohammed Plage, the top of the  $\delta^{13}\text{C}$  (the 'first peak') occurs in the middle of cycle 1. In cores S13, S57 and S75 this peak is seen at the transition between cycles 0 and 1. This difference of 1.5 obliquity cycles suggests ~60 kyrs is missing from the sedimentary record. Due to uncertainties in the exact positioning of the 'first peak' in Mohammed Plage, 50–80 kyrs is a safer estimate for the duration of the hiatus.

### 5.4. Organic carbon and organic matter composition

Total organic carbon content rhythmically fluctuates throughout the section (Fig. 2). However, a stepwise increase from base to top is observed as also noted in a previous study (Gebhardt et al., 2004). In the lower part of the section (0–8 m) TOC values fluctuate between 0–5% followed by more elevated values above 3–11%. A slight increase in TOC% is observed during the isotope excursion or plateau, although the highest value is observed just above the 'first peak' in  $\delta^{13}\text{C}$  values (10.7%).

Hydrogen and Oxygen Index (HI/OI) values display an inverse correlation and evolve in three distinct phases (Fig. 4). Phase 1 (0–8 m) shows a scattered, but easily identifiable increase in HI values, with

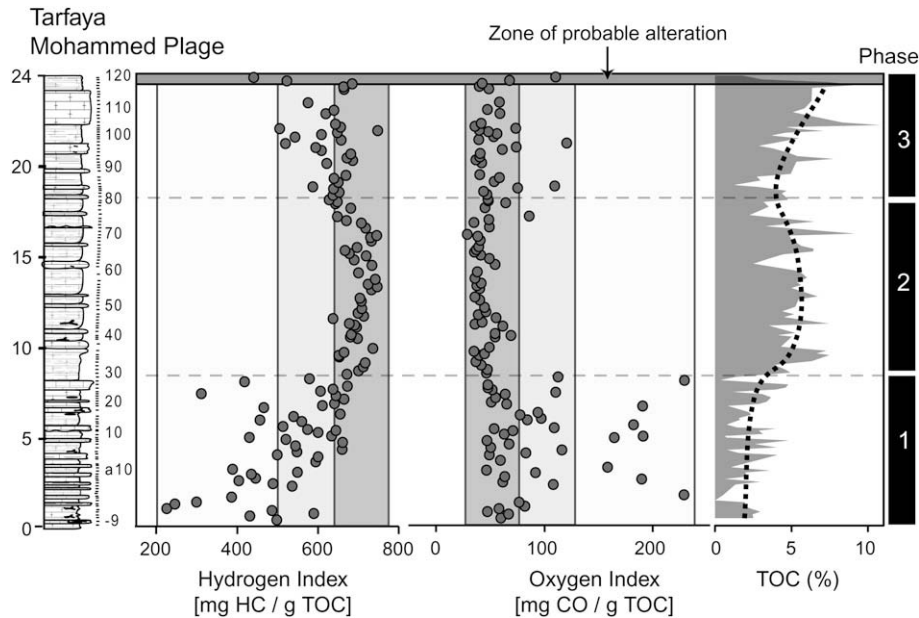


Fig. 4. Hydrogen index (HI) and oxygen index (OI) plotted against depth. The shaded rectangles represent degree of scatter, which are high in phases 1 and 3.

less scatter towards the top. A similar though inverse pattern is observed in OI values. Phase 2 marks a period of stability in both HI and OI values up to approximately 16 m. In Phase 3, HI values increasing scatter near the top of the section. HI and OI values broadly show inverse trends. The most accurate way to describe the evolution of HI and OI values is as a function of varying degrees of scatter. OI values show the least scatter of values with the majority of points within the minimum scatter zone (dark rectangle). However, HI shows very few values within the dark rectangle during phases 1 and 3. Despite this in phase 2, all HI values are within the dark rectangle.

A scatter plot between OI and HI (Fig. 5) shows type II organic matter (marine) dominant with the highest TOC contents associated with higher HI's and lower OI's. The lower HI values tend to be towards the base of the section. In this case low HI values are probably not indicative of greater continental organic matter input, but rather reflect effective oxygenation of the water column, which causes the degradation of marine organic matter, making it appear similar to type III (continental, see arrow in Fig. 5).

##### 5.5. Bulk rock mineralogy (0–24 m)

Quartz values fluctuate greatly at the base of the section and decrease steadily towards the top (Fig. 6). The lowest values occur above the isotope excursion (<2%). The detrital index (plotted against a logarithmic scale) also decreases gradually from the base to the top of the section, corresponding with the gradual increase in sea level (Gebhart et al., 2004). At the  $\delta^{13}\text{C}$  excursion, the detrital index shows increased fluctuation.

Calcite content remains high throughout the section, although the variability decreases considerably up-section. Between 0 and 7 m values vary from a high of 99% to a low of 20%. From 7 to 18 m calcite values remain above 70% and increase to above 85% from 18 to 24 m. There is a near perfect inverse relationship between calcite and quartz contents.

Phyllosilicate contents are more or less constant around 8 to 10% until MB 82 There is then a decrease to values of around 5%.

K-Feldspar content shows 3 distinct phases. In the lower part of the section (0–9 m), values remain mostly below 13%, but fluctuate greatly. In the middle part, (9–18.5 m) feldspar accumulation practically ceased (<5%). In the upper part of the section near the

$\delta^{13}\text{C}$  shift (21 m) there is an isolated peak of 10%. No K-Feldspar is observed above 22.5 m. Small spikes in plagioclase content are seen between 0 and 5 m (1.8%) and from 21 to 23 m (4–6%). Between 5 and 21 m there is total absence of plagioclase.

Ankerite content remains below 5% for the most of the section, but with a noticeable spike of 25% in the second sample from the base.

Secondary gypsum is relatively abundant at the base of the section reaching a maximum value of approximately 4% (Fig. 6). There is a complete absence of gypsum above 7.5 m, except near the top of the section (22–24 m) where it reaches 6%.

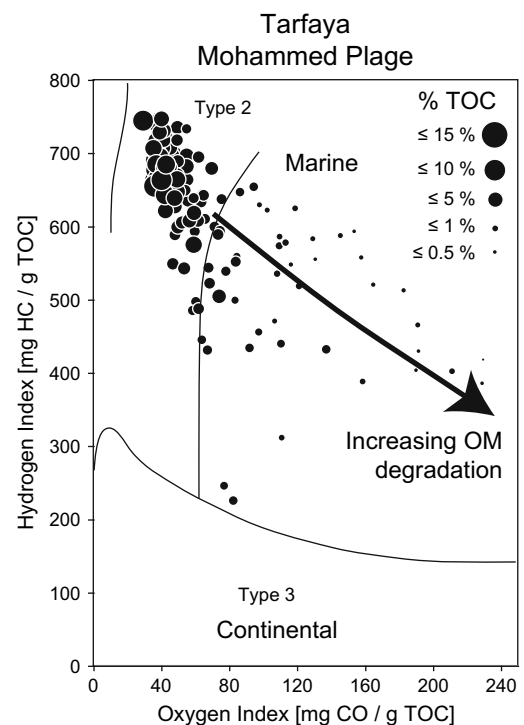


Fig. 5. HI/OI plot demonstrates that the dominant source of organic matter is of marine origin.

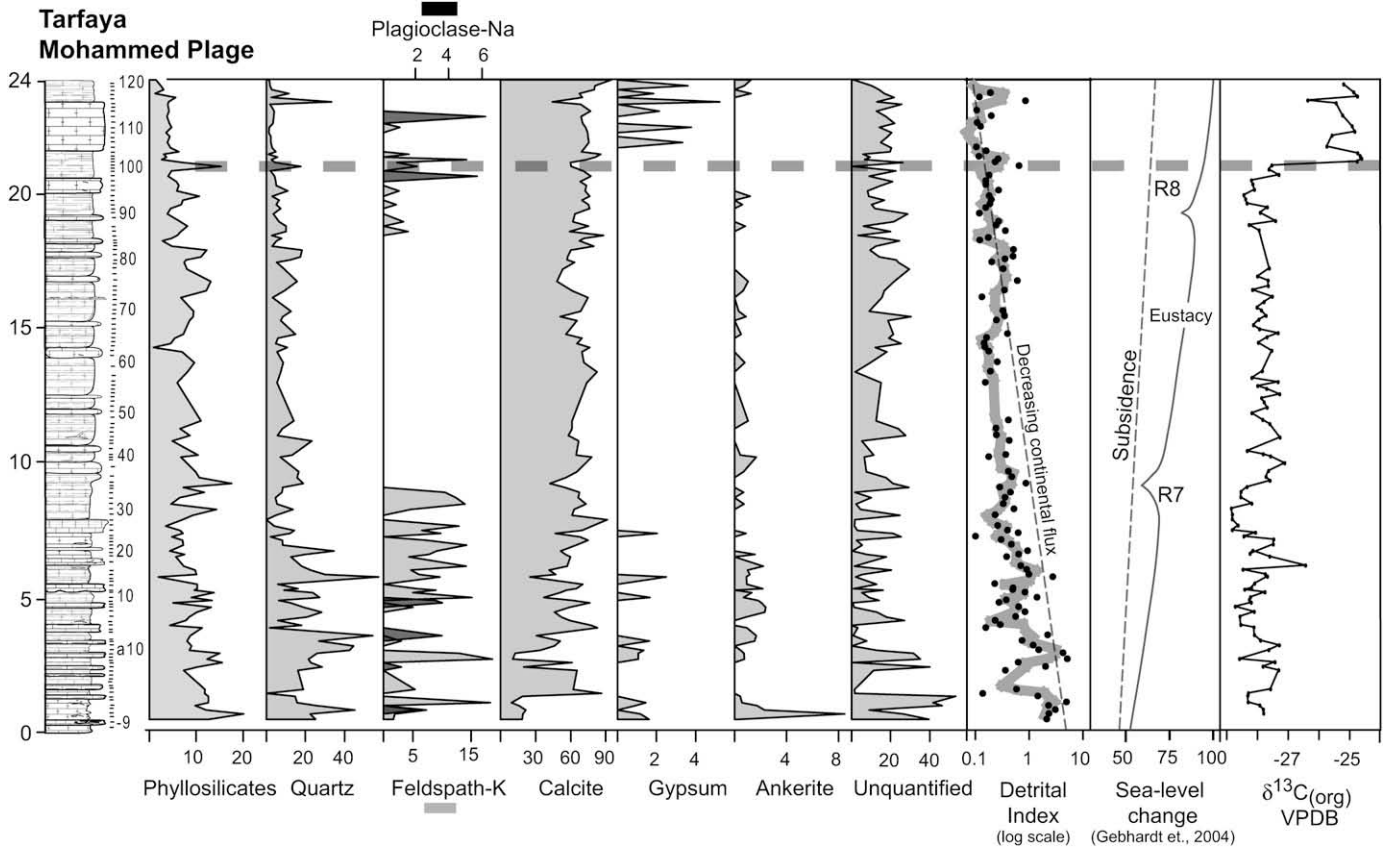


Fig. 6. Bulk rock mineralogy from XRD analysis with detrital index, relative sea-level curve (calculated using percentages of planktonic foraminifera by Gebhardt et al., 2004) and  $\delta^{13}\text{C}_{(\text{org})}$  data.

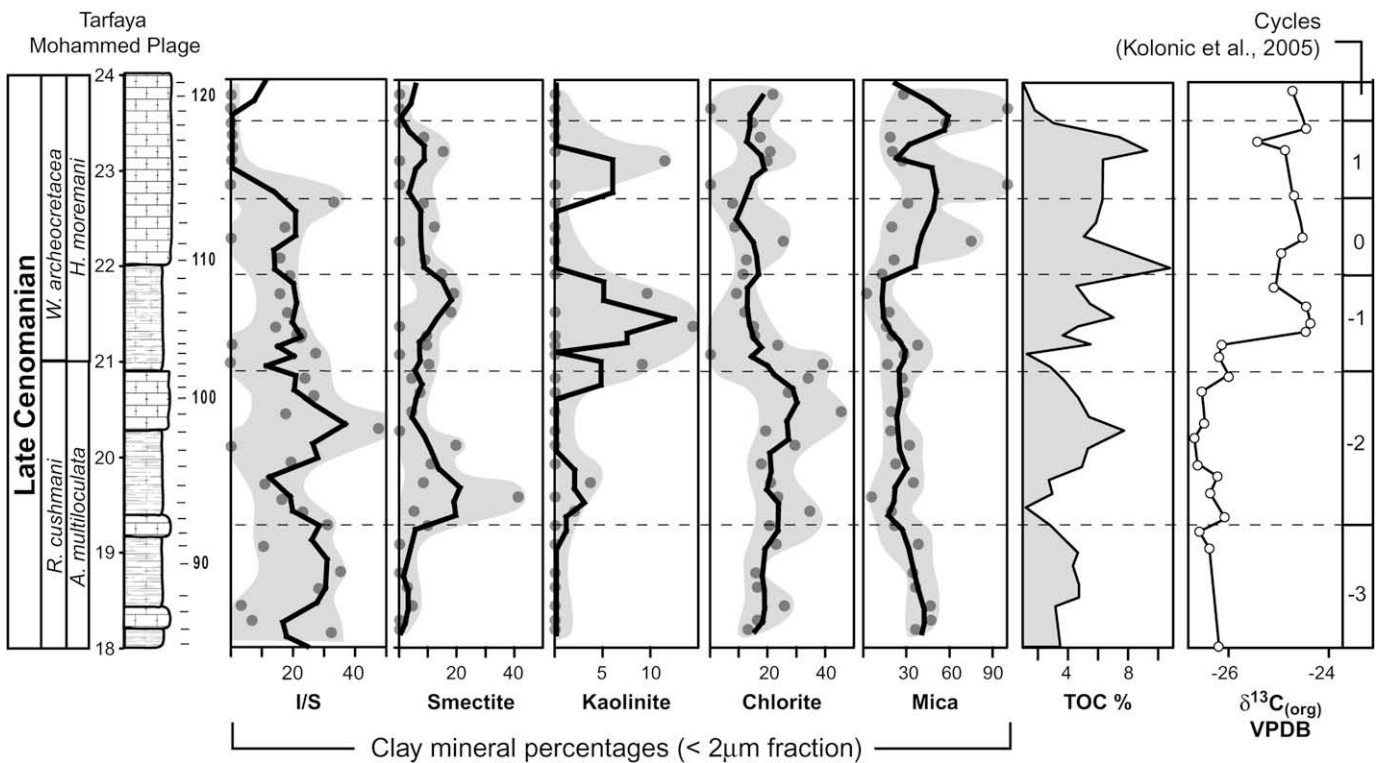
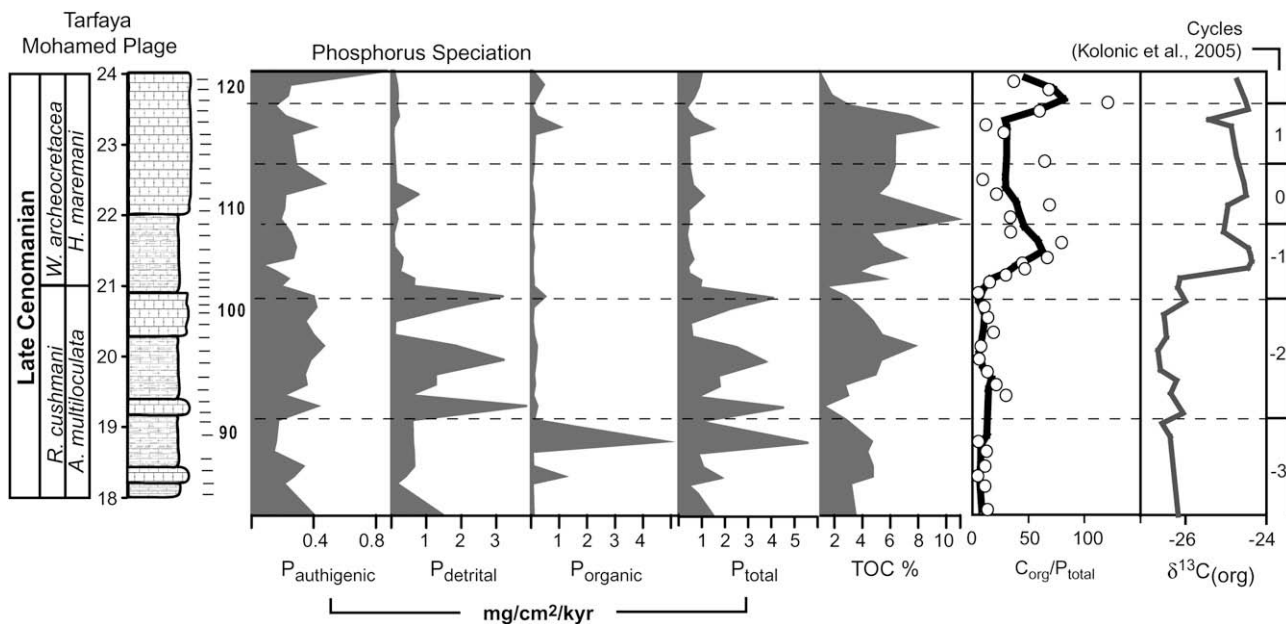


Fig. 7. Relative abundance of major clay minerals in the  $<2\ \mu\text{m}$  sediment fraction before and during OAE 2.



**Fig. 8.** Results from a sequential extraction of phosphorus (including  $P_{\text{authigenic}}$  apatite,  $P_{\text{detrital}}$  and  $P_{\text{organic}}$ ).  $P_{\text{reactive}}$  is taken as an addition of these phases.  $C_{\text{org}}/P_{\text{reactive}}$  (Redfield) ratios are also calculated and included alongside TOC and  $\delta^{13}\text{C}_{\text{(org)}}$  data.

### 5.6. Clay mineralogy (<2 $\mu\text{m}$ ) 18–24 m

Smectite percentages average around 10% for the top of the section with two samples at 19.6 and 20.1 m reaching 40% and 20% respectively (Fig. 7). There is a small increase at the onset of the isotope excursion (15%). Illite/smectite (I/S) ratios remain relatively constant at approximately 20% from 18 to 22.75 m and drop to zero above this interval. Kaolinite content is negligible throughout the section (including below 18 m: not shown), except for minor enrichments (<15%) at 19.75 m, 21 m and 23.1 m. Chlorite contents are generally higher between 18 and 21 m (20–30%), and drops below 20% at the onset of the  $\delta^{13}\text{C}$  excursion and for the remainder of the section. The fine fraction of mica is more abundant above the isotope excursion (>60%, as opposed to 30% before the excursion).

### 5.7. Phosphorus speciation and Redfield ratios (18–24 m)

There appear to be two phases of P accumulation in the Mohammed Plage section. Fig. 8 separates the lower part of the section (relatively abundant P accumulation) and the upper part (relatively depleted). The exception to this is  $P_{\text{authigenic}}$ , which remains relatively consistent (0.2–0.4  $\text{mg}/\text{cm}^2/\text{kyr}$ ) throughout the section. The switch between P-rich and P-poor sediments is coeval with the start of the positive  $\delta^{13}\text{C}$  shift and a re-introduction of higher TOC values.

There are some significant differences between the behaviour of the P phases. For example  $P_{\text{organic}}$  appears not to contribute significantly to the  $P_{\text{total}}$ , despite the high amount of organic matter. Only one sample (MB 90) registers a significant elevation in  $P_{\text{organic}}$  MARs (5  $\text{mg}/\text{cm}^2/\text{kyr}$ ). Otherwise, the values never exceed 1  $\text{mg}/\text{cm}^2/\text{kyr}$  and usually stay below 0.2  $\text{mg}/\text{cm}^2/\text{kyr}$ .  $P_{\text{detrital}}$  contributes most significantly to the  $P_{\text{total}}$  with 4 values above 2  $\text{mg}/\text{cm}^2/\text{kyr}$  prior to the isotope excursion.  $P_{\text{detrital}}$  fluctuates substantially up to this point before reducing to minimal values in the post-isotope excursion.

There is a sharp decrease in TOC values in the topmost samples (MB 119–121) preceding a 2-fold increase in  $P_{\text{authigenic}}$  ARs (MB 121). See Tables 1 and 2 for the P-speciation MAR data.  $C_{\text{org}}/P_{\text{total}}$  ratios increase substantially at the onset of the isotope excursion

and remain relatively high for the remainder of the section. The increase is from approximately 10 to 75, which is still considerably lower than the average value in today's oceans (~111).

**Table 1**

Phosphorus speciation data in mass accumulation rates for the Mohammed Plage Section

Depth (m)	Sample	$P_{\text{authigenic}}$	$P_{\text{detrital}}$	$P_{\text{organic}}$	$P_{\text{total}}$
Mass accumulation rate ( $\text{mg}/\text{cm}^2/\text{ka}$ )					
17.75	MB 82	0.40	1.48	0.08	1.96
18.2	MB 85	0.21	0.15	0.05	0.40
18.3	MB 86	0.27	0.40	1.18	1.85
18.45	MB 87	0.33	0.65	0.07	1.06
18.65	MB 88	0.14	0.64	0.06	0.84
18.8	MB 89	0.16	0.62	4.78	5.55
19.1	MB 90	0.17	0.60	0.10	0.87
19.3	MB 91	0.42	3.86	0.22	4.50
19.45	MB 92	0.20	0.51	0.07	0.78
19.6	MB 93	0.35	1.27	0.14	1.77
19.75	MB 94	0.34	1.27	0.10	1.72
19.95	MB 95	0.38	3.21	0.17	3.76
20.15	MB 96	0.46	1.85	0.20	2.51
20.3	MB 97	0.40	0.09	0.10	0.59
20.5	MB 98	0.35	0.11	0.06	0.51
20.7	MB 99	0.42	1.74	0.09	2.25
20.85	MB 100	0.40	3.18	0.49	4.07
21	MB 101	0.18	0.64	0.08	0.91
21.1	MB 102	0.24	0.66	0.08	0.97
21.2	MB 103	0.16	0.24	0.06	0.45
21.3	MB 104	0.07	0.29	0.05	0.40
21.4	MB 105	0.27	0.31	0.05	0.63
21.55	MB 106	0.29	0.08	0.10	0.47
21.75	MB 107	0.25	0.06	0.03	0.35
21.95	MB 108	0.19	0.17	0.09	0.45
22.1	MB 109	0.21	0.10	0.11	0.42
22.3	MB 110	0.22	0.78	0.09	1.08
22.45	MB 111	0.47	0.13	0.02	0.62
22.7	MB 112	0.29	0.11	0.08	0.47
23.15	MB 114	0.26	0.06	0.13	0.45
23.25	MB 115	0.41	0.07	1.03	1.51
23.4	MB 116	0.22	0.21	0.20	0.63
23.55	MB 117	0.15	0.16	0.03	0.33
23.7	MB 118	0.23	0.19	0.24	0.66
23.85	MB 119	0.25	0.16	0.46	0.87
24.05	MB 120	0.88	0.08	0.04	1.00

**Table 2**  
Major sediment phase elemental composition analysed via ICP-MS

Depth (meters)	Sample	Al	Ca	Ba	Ba*	K/Al	Ti/Al	Mg/Ca	Sr/Ca
		ppm			Ba/Al <sub>2</sub> O <sub>3</sub> × 15%	mol/mol		(mmol/mol)	
16.25	MB 74	251	155208	5.1	4518	23.78	0.060	26.97	10.87
16.40	MB 75	418	103826	5.1	2686	17.48	0.059	55.56	15.68
16.60	MB 76	300	120485	4.1	3009	18.37	0.068	51.82	15.85
16.75	MB 77	143	235693	15.6	24501	33.11	0.072	14.57	10.79
17.05	MB 78	158	174991	10.7	15195	28.52	0.072	21.04	12.33
17.30	MB 79	150	203978	13	19439	29.69	0.071	16.78	10.78
17.40	MB 80	300	143612	6.8	5039	19.04	0.076	27.44	13.56
17.50	MB 81	282	171545	12.5	9930	22.44	0.069	25.52	9.95
17.75	MB 82	175	211361	9.5	12153	30.93	0.068	18.96	10.62
17.90	MB 83	775	163744	11.6	3306	6.04	0.071	30.46	15.61
18.10	MB 84	500	203307	15.2	6779	15.97	0.061	27.12	8.55
18.20	MB 85	202	208734	10.4	11523	22.32	0.071	15.59	4.84
18.30	MB 86	193	215858	4.2	4835	24.32	0.073	14.45	6.61
18.45	MB 87	411	210917	6.5	3497	13.25	0.065	16.71	10.86
18.65	MB 88	447	199568	4.9	2405	12.16	0.068	17.75	13.22
18.80	MB 89	406	213211	6	3264	14.88	0.062	17.71	11.71
19.10	MB 90	474	188632	5.2	2407	16.67	0.057	28.61	10.03
19.30	MB 91	578	175499	12.9	4960	12.82	0.054	22.21	12.65
19.45	MB 92	379	153018	9.7	5697	19.31	0.068	28.43	10.80
19.60	MB 93	542	174613	12.7	5211	16.29	0.051	20.99	8.96
19.75	MB 94	736	172447	14	4218	10.67	0.055	28.80	9.57
19.95	MB 95	807	147862	14.1	3870	12.46	0.066	24.90	10.05
20.15	MB 96	341	197593	12.6	8252	14.47	0.094	16.73	7.66
20.30	MB 97	236	195963	12.8	12142	20.97	0.113	17.68	8.96
20.50	MB 98	131	235837	16.6	28450	23.55	0.078	11.36	6.78
20.70	MB 99	400	167070	14.4	8039	17.39	0.062	30.96	7.07
20.85	MB 100	398	208076	19.3	10849	12.94	0.066	17.35	8.76
21.00	MB 101	222	201344	24.1	24364	18.86	0.099	17.30	10.04
21.10	MB 102	437	187963	18.4	9412	12.03	0.081	17.95	13.08
21.20	MB 103	525	191058	16.4	6967	10.35	0.103	20.01	10.48
21.30	MB 104	244	225745	12.7	11650	16.20	0.098	15.16	9.73
21.40	MB 105	351	173168	15.4	9810	16.06	0.089	30.51	9.30
21.55	MB 106	688	194201	20.1	6512	8.99	0.128	24.75	4.33
21.75	MB 107	306	238189	11.7	8541	12.53	0.164	14.53	8.87
21.95	MB 108	292	219789	12.2	9339	13.20	0.202	15.56	9.80
22.10	MB 109	343	216777	12.1	7876	13.55	0.74	16.54	12.85
22.30	MB 110	614	176800	18.9	6864	10.30	0.75	29.21	13.44
22.45	MB 111	515	212276	14.1	6099	8.97	0.254	19.41	11.56
22.70	MB 112	292	183112	21.3	16351	19.04	0.157	22.88	8.15
22.90	MB 113	396	35115	10	5620	10.96	1.153	114.79	20.34
23.15	MB 114	218	213548	31.1	32037	31.56	0.116	20.38	10.20
23.40	MB 116	535	176236	14.7	6121	7.59	0.407	18.88	12.19
23.55	MB 117	696	152173	12.3	3915	11.45	0.066	42.44	21.08
23.70	MB 118	216	198869	13	13480	21.20	0.111	16.41	5.06
23.85	MB 119	235	186413	14.1	13439	31.90	0.086	24.83	4.78
24.05	MB 120	230	239296	19.1	18623	13.39	0.079	23.23	9.62

$P_{\text{detrital}}$  is susceptible to having been diagenetically transformed from  $P_{\text{authigenic}}$  (e.g. Filippelli and Delaney, 1995; Föllmi et al., 2005). It also in no way correlates with the detrital index described above. It is therefore reasonable, for the purposes of this study, to assume that the majority of measured  $P_{\text{detrital}}$  is recrystallized  $P_{\text{authigenic}}$  and thus was bioavailable. It is with this argument that  $P_{\text{detrital}}$  is included into the  $C_{\text{org}}/P_{\text{total}}$  ratio.

### 5.8. ICP-MS geochemistry

Fig. 9 shows the ICP-MS results for the carbonate fraction of the sediments between 17 and 24 m, encompassing the positive  $\delta^{13}\text{C}$  excursion.

Ba\* shows three periods of enrichment with values reaching 2200 ppm at 17 m, 2500 ppm at 20.5 m (immediately prior to the isotope excursion) and 3000 ppm at 23 m (during the excursion plateau). V/Al ratios are significantly enriched during the isotope excursion and for a short interval during the first stages of the isotope plateau reaching values of 0.2 (21.4–22 m). Above this interval, V/Al ratios decrease close to, but still above, pre-excursion values. Sr/Ca ratios remain stable through the samples analyzed, except for a minor exception during the isotope excursion at 22.5 m

where ratios increase from 0.08 to 0.2. The K/Al and Ti/Al ratio values are also stable, except for the top of the section (23–24 m) where they increase significantly.

## 6. Discussion

### 6.1. Long-term depositional history

The increase in TOC values from the base of the Mohammed Plage section and stable  $\delta^{13}\text{C}$  values (Fig. 2) suggest that productivity was not the primary control on OC accumulation. Gebhardt et al. (2004) drew the same conclusion pointing to the oxygen minimum zone impingement on shelf seas during sea-level highstands as the primary reason for the inhibition of organic matter oxidation. The gradual increase in HI values (phase 1, Fig. 4) could support this explanation, if they were caused by an increase in organic matter of marine origin and/or better preservation of organic matter. A shift from a continental to marine influence is also indicated by the decrease and increase in quartz and calcite values respectively (Fig. 6). A gradual increase in sea-level is perhaps best indicated by the gradual decrease in the detrital index (Fig. 6), which suggests a gradual decrease in terrigenous input and/or

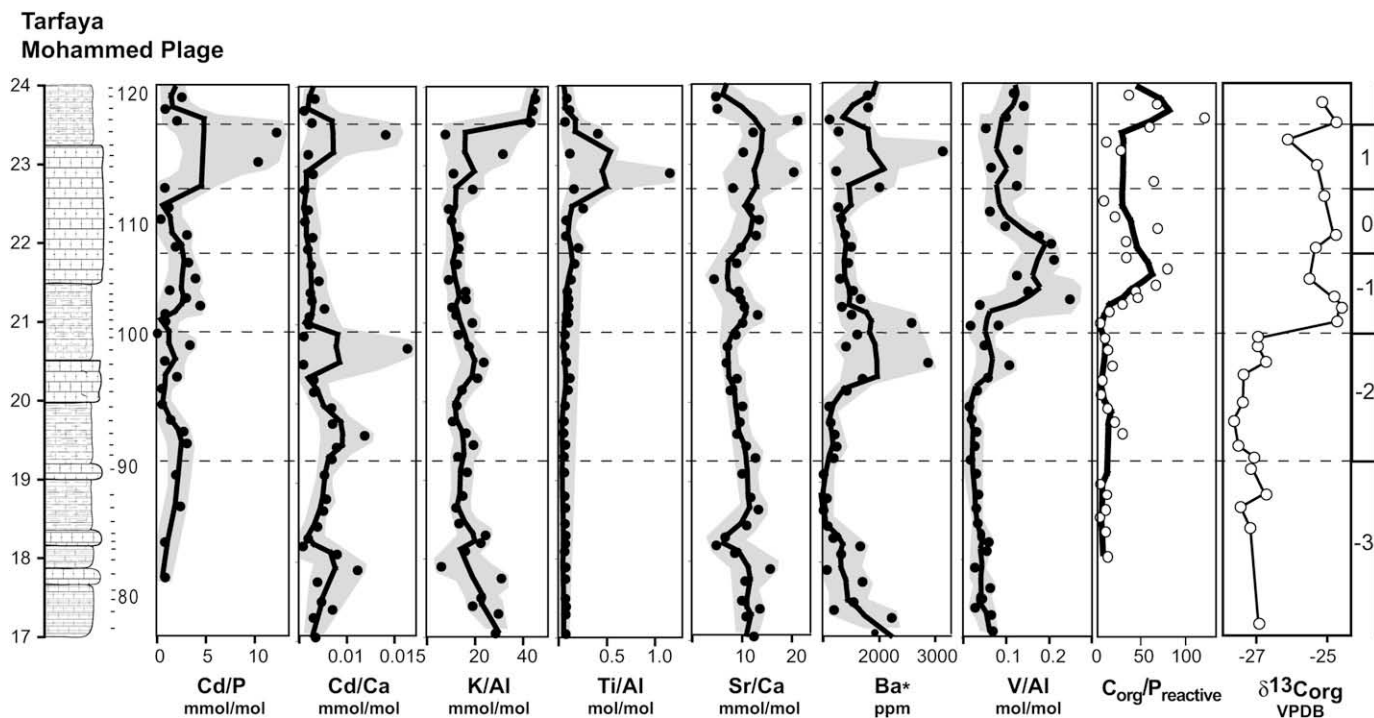


Fig. 9. ICP-MS data from the carbonate fraction of the sediment.

a rising sea-level, greater paleodepth and increased dilution of the terrigenous material. In the upper part of the section, the thinly laminated siltstones and marly limestone beds with horizontally aligned foraminifera also suggest low energy currents consistent with a higher sea level. The decrease in the frequency of siltstone beds from the bottom to the top of the section also supports this interpretation.

The small positive isotope excursion, shortly followed by a trough in sample MB 18 (Fig. 2) may represent the so-called 'mid-Cenomanian event' (MCE) (Coccioni and Galeotti, 2003). See above.

As noted above, the Tarfaya paleo-coast is widely regarded as having had a major upwelling cell offshore (Bush and Philander, 1997; Gustafsson et al., 2003). This interpretation is supported by the quantification of different phosphorus phases. For example,  $P_{\text{authigenic}}$  behaves differently compared to other P phases in that it is relatively constant throughout the section. This observation is consistent with a reliable upwelling zone, which provides abundant nutrients including dissolved inorganic P, which can then precipitate onto pellets, skeletal material or other binding sites forming  $P_{\text{authigenic}}$  (Van Cappellen and Ingall, 1994; Mackenzie et al., 1998). However, out of all the phases  $P_{\text{authigenic}}$  is the least abundant, despite the favourable upwelling zone environment. These lower than expected values may be symptomatic of the higher relative sea level in the upper-part of the section, which caused the OMZ to encroach further onto the continental shelf and thus resulted in a consistent, but limited, accumulation rate of  $P_{\text{authigenic}}$  due to lower oxygen availability.

## 6.2. Oceanic Anoxic Event 2

Immediately prior to the isotope excursion there is a noticeable enrichment in  $Ba^*$  in two samples (~20.5 m) coincident with a small peak in species richness (Figs. 3 and 9). The increase in biodiversity is primarily due to the temporary reintroduction of less common planktonic foraminifera which make an appearance

precisely at the  $\delta^{13}C$  excursion onset (e.g. *P. gibba*, *P. praehelvetica*, *D. imbricata* and *D. hagni*). Together with the disappearance of *R. cushmani* and *R. greenhornensis* in short succession of one another, this points to a time of maximum faunal turnover, which also marks the start of some profound geochemical changes in the sediments, for example, the coeval enrichment of Cd/Ca values with  $Ba^*$ . The Cd/P ratio is used as a proxy for sea-surface phosphate utilization due to the constant fractionation of P relative to Cd in primary productivity (Rickaby and Elderfield, 1999; Elderfield and Rickaby, 2000). These authors performed their analyses on planktonic foraminifera, whereas we use bulk-rock measurements, which provide less sensitive values. Nevertheless, our results suggest that the role of Cd as a micronutrient became significant for a short time (this is only seen in one sample) at the excursion onset. At this point, P MAR values drop considerably along with the Cd/Ca ratio. This may have been caused by an increase in dissolved inorganic phosphate (DIP) in the water column as a result of P recycling from sediments overlain by oxygen-depleted waters.

V/Al values show a similar trend as the positive  $\delta^{13}C$  excursion before reducing to values still elevated relative to pre-OAE 2 values (Fig. 9).  $P_{\text{detrital}}$  and  $P_{\text{organic}}$  contents almost completely disappear from the sediment and the average  $P_{\text{reactive}}$  AR is reduced by approximately 3 times. This transition is marked by a considerable drop in planktonic foraminiferal diversity and an increase in the opportunistic low oxygen tolerant species *H. moremani*, both suggesting a period of biotic stress. The increased V/Al and biotic stress combined with the decrease in P MARs is further evidence that oxygen depletion was crucial in limiting P accumulation.

The sharp increase in the  $C_{\text{org}}/P_{\text{reactive}}$  ratio at the excursion onset is also a good indication that phosphorus was being lost and/or prevented from accumulating in sediments. Given that the Tarfaya Basin is an upwelling region with an apparently strong biopump (Gustafsson et al., 2003), it would seem likely that this excess DIP could have become reintroduced into surface waters, stimulating further primary productivity. The trend to minimal P

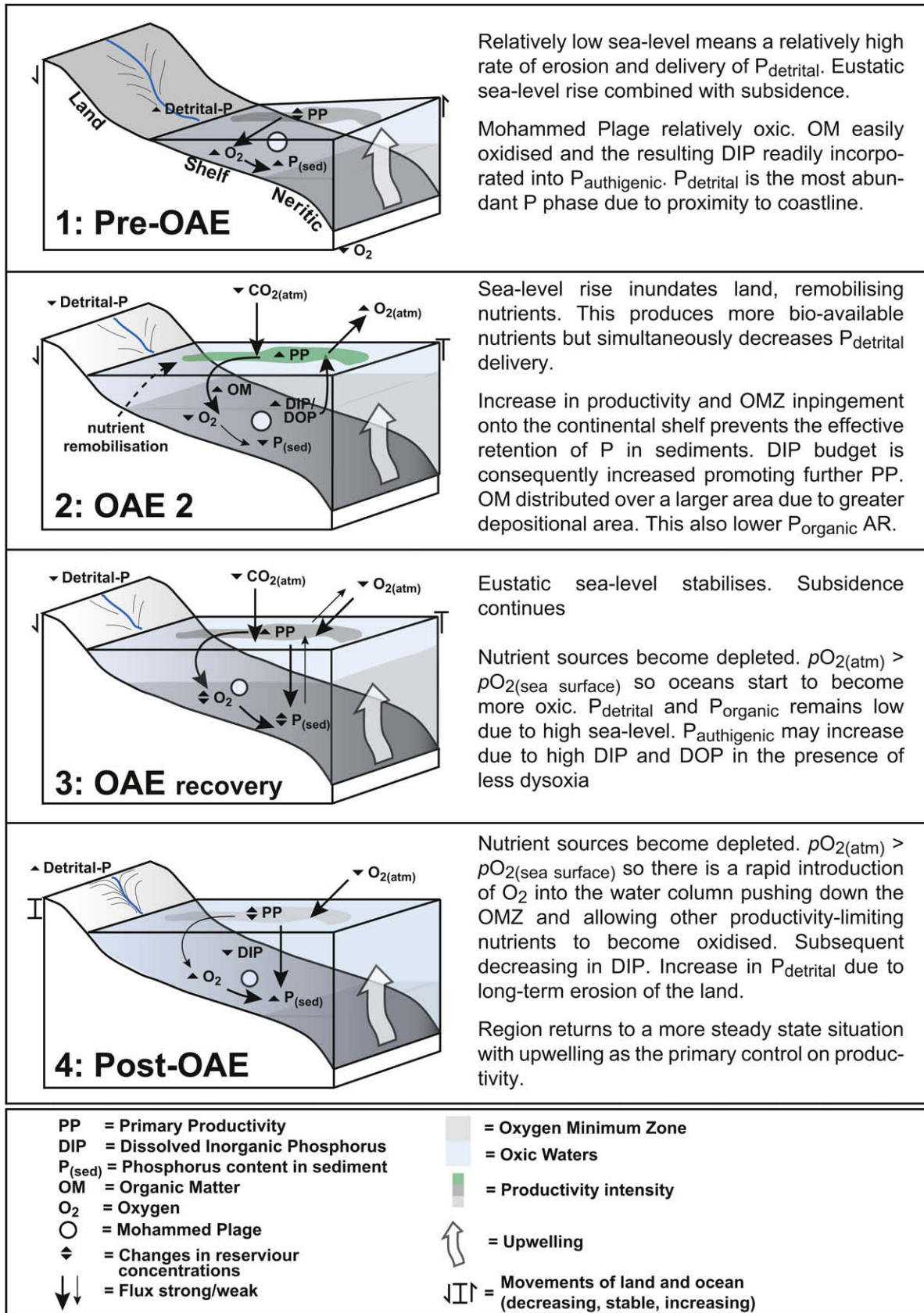


Fig. 10. Conceptual model outlined in the discussion.

retention during OAE2 has been shown in earlier compilations of oceanic P-burial rates (Föllmi, 1995, 1996; Föllmi et al., 2004; Nederbragt et al., 2004), and its link with anoxic conditions has been proposed by (Ingall and Van Cappellen, 1990; Ingall et al., 1993; Ingall and Jahnke, 1994; Van Cappellen and Ingall, 1994, 1996).

If increased DIP acted as a driver for productivity, this would have caused the continued formation of biogenic barite (for which  $Ba^*$  is used as a proxy in this study). However, our data shows only a brief increase in  $Ba^*$  formation prior to the  $\delta^{13}C$  excursion onset.  $Ba^*$  formation appears restricted within the isotope plateau despite almost certainly representing high productivity in this interval. This is probably due to a drop in barite production due to an oxygen deficient water column (Dickens, 2001; Castellini et al., 2006).

What caused these changes? Sea levels appear to have been increasing steadily for several million years prior to the isotope excursion onset. Although this leaves climate change as an obvious choice, there is little evidence to suggest that there was an increase in humidity or weathering. Two proxies could conceivably be called upon to infer an increase in continental input. OI's (Fig. 4) becomes slightly more scattered at the top of the section, suggesting a fluctuation in the abundance of continentally derived OM or more likely the hydraulic alteration via water percolating through the overlying Miocene grainstones. However, in the same samples we see elevated gypsum intensity values. We may assume that the gypsum does not represent dry conditions, but rather the conversion of pyrite ( $FeS_2$ ) into gypsum ( $CaSO_4(OH)$ ) via OM remediation. This is more likely to account for the observed decrease in OI values.

Clay minerals maybe used to infer more humid or arid conditions (Singer, 1984; Lu et al., 1998; Bolle et al., 2000; Bolle and Adatte, 2001). Kaolinite increases at the  $\delta^{13}C$  onset, but values do not exceed 15% (seen in one sample). The inferred increase in humidity and continental weathering from a 15% abundance in kaolinite is unlikely to have had a significant impact on productivity. A more likely source for the small increase in kaolinite at the  $\delta^{13}C$  excursion onset is a relatively rapid sea-level transgression, which results in reworking of sediments that were previously existed on dry land (Fig. 10). This idea was earlier proposed by (Hilbrecht et al., 1996). Gebhardt et al. (2004) used planktonic foraminifera to calculate a brief regression followed by a transgression prior to the excursion onset (Fig. 6). This may well have increased productivity by remobilising nutrients. In addition, the most dominant clay minerals in Mohammed Plage are smectite and mica, which point to a drier climate where sediments would have been more susceptible to reworking and erosion by the encroaching sea. The inundation of dry land would have had other effects. The elevated base level of rivers and the corresponding reduction in erosional capacity probably reduced  $P_{detrital}$  MARs (Fig. 8). Lower  $P_{organic}$  values may have resulted from OC deposition occurring over a larger shelf area.

A more expansive shallow sea has a greater ability to produce the oxidative regeneration of nutrients (Schlanger and Jenkyns, 1976; Jenkyns, 1980) creating a region of high primary productivity. Therefore, a shallow sea, especially in an upwelling area with abundant nutrients, such as the Tarfaya basin, was probably pre-disposed to becoming dysoxic.

The mode of OC accumulation appears to have changed during and after the  $\delta^{13}C$  excursion. Fluctuations in TOC may partly be orbitally controlled. The boundary between the finish and start of the 39 ka obliquity cycles from Kuhnt et al. (1997) (Fig. 8) coincides reasonably well with periods of minimum OC content. The base of the isotope  $\delta^{13}C$  excursion coincides with a transition from obliquity cycle  $-2$  to  $-1$  and the corresponding minimum in TOC. TOC values begin to rise, but not as rapidly as  $\delta^{13}C$  values.

### 6.3. Phosphorus recycling during OAE 2: A global phenomenon?

Nederbragt et al. (2004) modelled the behaviour of P under anoxic conditions, concluding that a change in the oceanic phosphorus cycle was the most realistic way to generate a substantial positive  $\delta^{13}C$  excursion. In the same study, empirical data from the Tarfaya drill hole S13 was presented. A decrease in weight % total phosphate at the onset of OAE 2's positive carbon isotope excursion was observed, as was an increase in  $C_{org}/P_{reactive}$  molar ratios (Fig. 11). Other recent studies (Mort et al., 2007a,b) show the same correlation in four other localities (the Pueblo CT GSSP, Colorado; Eastbourne, UK; Furlo, Italy; Manilva, Spain). These studies also used MARs calculated from isotopic, biostratigraphic and cyclostratigraphic datasets. Fig. 12 illustrates a correlation between the Mohammed Plage's  $\delta^{13}C$  and  $P_{reactive}$  AR curves and those of the 4 sections. Because the drop in P MAR is coevally observed in such a diversity in palaeoenvironments, it is very likely that this signature, if interpreted correctly, represents a critical factor in the processes that lead to the development of OAE 2.

### 6.4. Termination of OAE 2

The termination of OAE 2 is not documented in the sediments at Mohammed Plage. In previous studies, the final phase of OAE 2 seems to have occurred in the early Turonian with the rapid radiation of deep water agglutinated foraminifera (Kuhnt, 1992) indicating a return to more oxygenated waters (Kolonic et al., 2005). Eight species of planktonic foraminifera disappear at or during the  $\delta^{13}C$  excursion (precise location is uncertain due to probable hiatus) and reappear later, signalling the end of *maximum* environmental stress (Fig. 3).  $C_{org}/P_{reactive}$  ratios also decrease somewhat during this recovery phase, pointing to regional water column dysoxia as an important control on species abundance. However the fall in the  $C_{org}/P_{reactive}$  ratio is not due to an increase in P content, but rather a decrease in OC content due to degradation (see below).

TOC values reach their maximum during OAE 2, but are still highly variable, suggesting a degree of Milankovitch modulation. Alternatively, the proximity of Mohammed Plage to the paleo-coastline (albeit at a deep paleodepth) makes it an effective recorder of local changes in OC flux from continental sources. OI values fluctuate in the upper part of the section (phase 3, Fig. 4), thus suggesting fluctuations in the delivery of continental organic

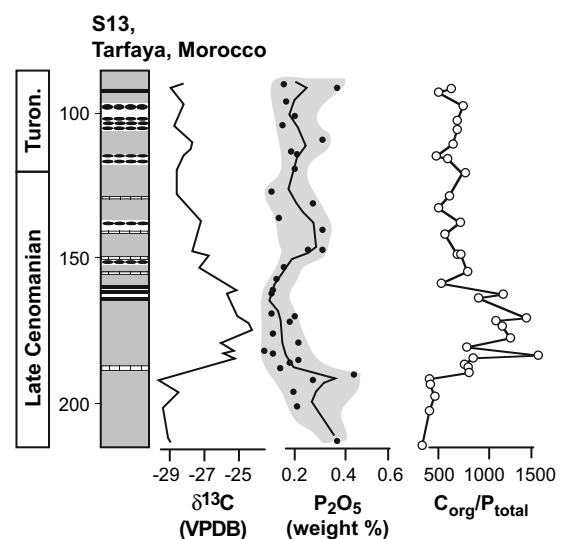
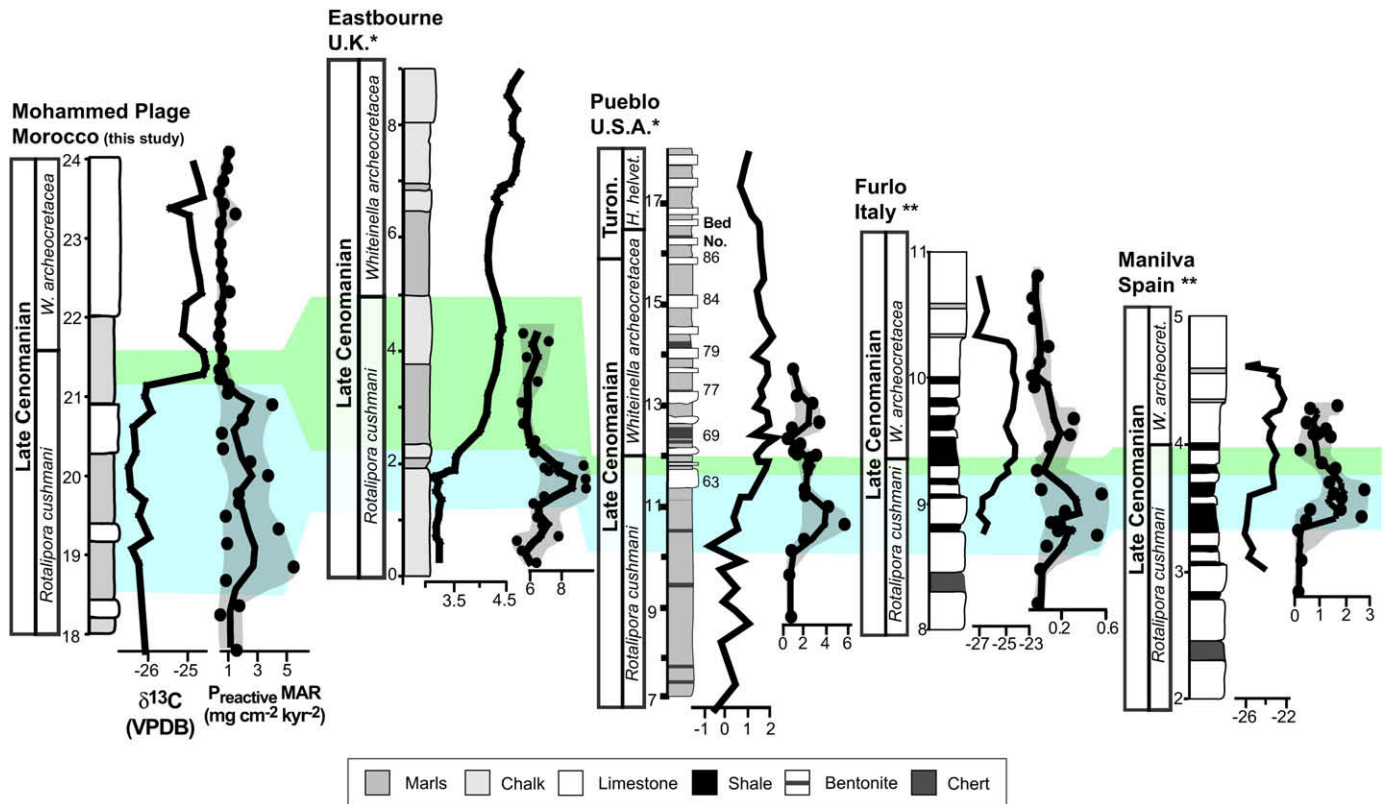


Fig. 11. A comparison of the Phosphate and  $C_{org}/P_{total}$  from drill hole S13, also in the Tarfaya basin. Modified after Nederbragt et al. (2004).



**Fig. 12.** Correlation of phosphorus mass accumulation rates with four other sections (3 from Europe and 1 from the Cenomanian-Turonian GSSP in Pueblo, Colorado). \*(Mort et al., in press). Lithology for Mohammed Plage has been simplified to conform with other lithologies presented. Lighted shaded area highlights the main phase of P accumulation, prior to and during the isotope excursion. The dark shaded area covers the fall in P accumulation until the extinction of *Rotalipora cushmani*. During and after this time, it is likely that dysoxia had reduced the nutrient retention ability of the sediment thus causing the recycling of P.

matter or oxygenation. However, the overlying porous Miocene deposits may have been conducive to the percolation of water in the highest Cenomanian bed resulting in its alteration. This is a more convincing explanation for the dramatic fall in TOC percentages in the uppermost samples, although not the increased in  $P_{\text{authigenic}}$ . Due to these types of complications, it is very difficult to identify with certainty any precursors to the end of OAE 2.

## 7. Conclusions

OAE 2 is a global phenomenon and its overall cause must therefore also be global in scale. The event is represented (at least partially) in the Mohammed Plage section by a  $+2.5\text{‰}$  shift in  $\delta^{13}\text{C}$  values, marking the regional expression of this global event. There is no direct evidence to link events in this area of the Tarfaya basin to the direct cause of OAE 2 itself. However, it is possible to conclude that the long-term eustatic sea-level rise and subsidence resulted in a large shallow continental shelf sea, which combined with an abundant nutrient source (provided by upwelling) made this area susceptible to dysoxia via global mechanisms that caused OAE 2 (e.g., sea level change, upwelling).

Mohammed Plage shows a distinct long-term deepening trend, which was caused by a mixture of sea-level rise and shelf subsidence. This is seen in decreases in quartz, phyllosilicates and feldspar, increases in quartz and a corresponding fall in detrital and organic matter indices.

OAE 2 is clearly expressed by an abrupt  $+2.5\text{‰}$  shift in  $\delta^{13}\text{C}$  values. A rapid sea-level rise, superimposed on the long-term rise may have leached continentally stored nutrients, stimulated productivity, created bottom dysoxia and prevented the accumulation

of P through the expansion and intensity of the OMZ. This may have led to regeneration of P and other redox-sensitive nutrients. Nutrients recycled would have increased the DIP content of the water, further sustaining primary productivity. If this interpretation is correct, then the global significance of this mechanism is apparent when compared to other OAE 2 phosphorus studies in the Tarfaya basin and in sections from Europe and America (Figs. 11 and 12). Productivity would have produced more atmospheric  $\text{O}_2$  simultaneously drawing down  $\text{CO}_2$  from the atmosphere. Eventually the abundance of  $\text{O}_2$  in the atmosphere may have acted as a negative feedback to halt the cycle of productivity–anoxia–P recycling–productivity. Once nutrient supply fell (due to consumption and burial and/or fall in supply) this would have led to a return of more oxygenated bottom waters and a termination to OAE 2.

The primary contribution of this data is that it has added considerable weight to previous authors work on both the long-term depositional history of the Tarfaya Basin and by providing significant new geochemical information and insights into the events and mechanisms that took place immediately before and during OAE 2.

## Acknowledgements

This report is based upon work supported by the Swiss National Fund No. FN21-67702.02 (TA), the US National Science Foundation under Grant NSF INT 0115357 (GK), and the German Science Foundation grant STU 169/10-1 to 3 (DS).

## References

Adatte, T., Stinnesbeck, W., Keller, G., 1996. Lithostratigraphical and mineralogic correlations of near K/T boundary clastic sediments in northeastern Mexico:

- implications for origin and nature of deposition. *Geological Society of America Special Paper* 307, 211–226.
- Aguilera-Franco, N., Hernandez-Romano, U., Allison, P.A., 2001. Biostratigraphy and environmental changes across the Cenomanian-Turonian boundary, southern Mexico. *Journal of South American Earth Sciences* 14, 237–255.
- Anderson, D.L., Delaney, M.L., 2000. Sequential extraction and analysis of phosphorus in marine sediments: streamlining of the SEDEX procedure. *Limnology and Oceanography* 45, 509–515.
- Attewell, P.B., Farmer, I.W., 1976. *Principles of Engineering Geology*. Chapman and Hall, London.
- Bolle, M.-P., Adatte, T., 2001. Palaeocene-early Eocene climate evolution in the Tethyan realm: clay mineral evidence. *Clay Minerals* 36, 249–261.
- Bolle, M.-P., Tantawy, A.A., Pardo, A., Adatte, T., Burns, S.J., Kassab, A., 2000. Climatic and environmental changes documented in the upper Paleocene to lower Eocene of Egypt. *Eclogae Geologicae Helveticae* 93, 33–51.
- Bush, A.B.G., Philander, S.G.H., 1997. The late Cretaceous: simulation with a coupled atmosphere-ocean general circulation model. *Paleoceanography* 12, 495–516.
- Castellini, D.G., Dickens, G.R., Snyder, G.T., Ruppel, C.D., 2006. Barium cycling in shallow sediment above active mud volcanoes in the Gulf of Mexico. *Chemical Geology* 1, 1–30.
- Cocconi, R., Galeotti, S., 2003. The mid-Cenomanian Event: prelude to OAE 2. *Palaeogeography, Palaeoclimatology, Palaeoecology* 190, 427–440.
- Dickens, G.R., 2001. Sulphate profiles and barium fronts in sediment on the Blake Ridge: present and past methane fluxes through large gas hydrate reservoir. *Geochimica et Cosmochimica Acta* 65, 529–543.
- Eijsink, L.M., Krom, M.D., de Lange, G.J., 1997. The use of sequential extraction techniques for sedimentary phosphorus in eastern Mediterranean sediments. *Marine Geology* 139, 147–155.
- El Albani, A., Kuhnt, W., Luderer, F., Herbin, J.P., Caron, M., 1999a. Palaeoenvironmental evolution of the late Cretaceous sequence in the Tarfaya Basin (southwest of Morocco). In: Cameron, N.R., Bate, R.H., Clure, V.S. (Eds.), *The Oil and Gas Habitats of the South Atlantic*, 153. Geological Society of London, Special Publication, pp. 223–240.
- El Albani, A., Vachard, D., Kuhnt, W., Chellia, E.H., 1999b. Signature of hydrodynamic activity caused by rapid sea level changes in pelagic organic rich sediments, Tarfaya Basin (southern Morocco). *Science de la Terre et Planetes* 329, 397–404.
- Elderfield, H., Rickaby, R.E.M., 2000. Oceanic Cd/P ratio and nutrient utilization in the glacial Southern Ocean. *Nature* 405, 305–310.
- Espitalié, J., Deroo, G., Marquis, F., 1985. La pyrolyse Rock-Eval et ses applications. *Revue de l'Institut Français du Pétrole* 40, 563–579.
- Filippelli, G.M., Delaney, M.L., 1995. Phosphorus geochemistry, diagenesis, and mass balances of the Miocene Monterey Formation at Shell Beach, California. *United States Geological Survey Bulletin* (1995), 1–11. Special publication F, G.
- Föllmi, K.B., 1995. 160 m.y. record of marine sedimentary phosphorus burial: coupling of climate and continental weathering under greenhouse and icehouse conditions. *Geology* 23, 859–862.
- Föllmi, K.B., 1996. The phosphorus cycle, phosphogenesis, and marine phosphate-rich deposits. *Earth-Science Reviews* 40, 55–124.
- Föllmi, K.B., Tamburini, F., Hosein, R., van de Schootbrugge, B., Arn, K., Rambeau, C., 2004. Phosphorus, a servant faithful to Gaia? Biosphere remediation rather than regulation. In: Schneider, S.H., Miller, J.R., Crist, E., Boston, P. (Eds.), *Scientists Debate Gaia: The Next Century*. MIT Press, Cambridge, Massachusetts, pp. 79–92.
- Föllmi, K.B., Badertscher, C., de Kaemel, E., Stille, P., John, C., Adatte, T., Steinmann, P., 2005. Phosphogenesis and organic-carbon preservation in the Miocene Monterey Formation at Naples Beach, California – the Monterey hypothesis revisited. *Geological Society of America Bulletin* 117, 589–619.
- Gale, A.S., Jenkyns, H.C., Kennedy, W.J., Corfield, R.M., 1993. Chemostratigraphy versus biostratigraphy – data from around the Cenomanian-Turonian boundary. *Journal of the Geological Society, London* 150, 29–32.
- Gebhardt, H., 1999. Cenomanian to Coniacian biogeography and migration of North and West African ostracods. *Cretaceous Research* 20, 215–229.
- Gebhardt, H., Kuhnt, W., Holbourn, A., 2004. Foraminiferal response to sea level change, organic flux and oxygen deficiency in the Cenomanian of the Tarfaya Basin, southern Morocco. *Marine Micropalaeontology* 53, 133–157.
- Gräfe, K.U., 2002. Stratigraphische Korrelation und Steuerungsfaktoren sedimentärer Zyklen in ausgewählten borealen und tethyalen Becken des Cenoman/Turon Europas und Nordwestafrikas. *Berichte aus dem Fachbereich der Geowissenschaften, Universität Bremen* 198, 1–197.
- Gustafsson, M., Holbourn, A., Kuhnt, W., 2003. Changes in Northeast Atlantic temperature and carbon flux during the Cenomanian/Turonian paleoceanographic event: the Goban Spur stable isotope record. *Palaeogeography, Palaeoclimatology, Palaeoecology* 201, 51–66.
- Hallam, A., Wignall, P.B., 1999. Mass extinctions and sea-level changes. *Earth-Science Reviews* 48, 217–250.
- Haq, B.U., Hardenbol, J., Vail, P.R., 1987. Chronology of fluctuating sea levels since the Triassic. *Science* 235, 1156–1167.
- Hilbrecht, H., Frieg, C., Troger, K.A., Voigt, S., Voigt, T., 1996. Shallow water facies during the Cenomanian-Turonian anoxic event: bio-events, isotopes, and sea level in southern Germany. *Cretaceous Research* 17, 229–253.
- Holbourn, A., Kuhnt, W., 2002. Cenomanian-Turonian paleoceanographic change on the Kerguelen Plateau: a comparison with Northern Hemisphere records. *Cretaceous Research* 23, 333–349.
- Holbourn, A., Kuhnt, W., El Albani, A., Ly, A., Gomez, R., Herbin, J.P., 1999. Palaeoenvironments and palaeobiogeography of the Late Cretaceous Casamance transect (Senegal, NW Africa): distribution patterns of benthic foraminifera, organic carbon and terrigenous flux. *Neues Jahrbuch für Geologie und Paläontologie, Abhandlungen* 212, 335–377.
- Ingall, E., Jahnke, R., 1994. Evidence for enhanced phosphorus regeneration from marine-sediments overlain by oxygen depleted waters. *Geochimica et Cosmochimica Acta* 58, 2571–2575.
- Ingall, E.D., Bustin, R.M., Van Cappellen, P., 1993. Influence of water column anoxia on the burial and preservation of carbon and phosphorus in marine shales. *Geochimica et Cosmochimica Acta* 57, 303–316.
- Ingall, E.D., Van Cappellen, P., 1990. Relation between sedimentation-rate and burial of organic phosphorus and organic carbon in marine sediments. *Geochimica et Cosmochimica Acta* 54, 373–386.
- Jeans, C.V., Long, D., Hall, M.A., Bland, D.J., Cornford, C., 1991. The geochemistry of the Plenus Marls at Dover, England – evidence of fluctuating oceanographic conditions and of glacial control during the development of the Cenomanian-Turonian delta-C-13 Anomaly. *Geological Magazine* 128, 603–632.
- Jenkyns, H.C., 1980. Cretaceous anoxic events, from continents to oceans. *Journal of the Geological Society, London* 137, 171–188.
- Jenkyns, H.C., 1991. Impact of Cretaceous Sea-Level Rise and Anoxic Events on the Mesozoic Carbonate Platform of Yugoslavia. *American Association of Petroleum Geologists Bulletin* 75, 1007–1017.
- Keller, G., Han, Q., Adatte, T., Burns, S.J., 2001. Palaeoenvironment of the Cenomanian-Turonian transition at Eastbourne, England. *Cretaceous Research* 22, 391–422.
- Keller, G., Pardo, A., 2004. Age and paleoenvironment of the Cenomanian-Turonian global stratotype section and point at Pueblo, Colorado. *Marine Micropalaeontology* 51, 95–128.
- Keller, G., Berner, Z., Adatte, A., Chellai, E.H., Stüben, D. Oceanic Events and Biotic Effects of the Cenomanian-Turonian Anoxic Event, Tarfaya Basin, Morocco. *Cretaceous Research*, in press.
- Kolonic, S., Sinninghe Damsté, J.S., Bottcher, M.E., Kuypers, M.M.M., Kuhnt, W., Beckmann, B., Scheeder, G., Wagner, T., 2002. Geochemical characterization of Cenomanian/Turonian black shales from the Tarfaya Basin (SW Morocco) – relationships between palaeoenvironmental conditions and early sulphurization of sedimentary organic matter. *Journal of Petroleum Geology* 25, 325–350.
- Kolonic, S., Wagner, T., Forster, A., Sinninghe Damsté, J.S., et al., 2005. Black shale deposition on the northwest African shelf during the Cenomanian/Turonian oceanic anoxic event: climate coupling and global organic carbon burial. *Paleoceanography* 20, 1006, doi:10.1029/2003PA000950.
- Kübler, B., 1987. Cristallinité de l'illite, méthodes normalisées de préparations, méthodes normalisées de mesures. 1. *Cahier Insitut de Géologie*, 13.
- Kuhnt, W., 1992. Abyssal recolonization by benthic foraminifera after the Cenomanian-Turonian boundary anoxic event in the north-Atlantic. *Marine Micropalaeontology* 19, 257–274.
- Kuhnt, W., Chellai, E.H., Holbourn, A., Luderer, F., Thurow, J., Wagner, T., El Albani, A., Beckmann, B., Hervin, J.-P., Kawamura, H., Kolonic, S., Nederbragt, A., Street, C., Ravilliois, K., 2001. Morocco basin's sedimentary record may provide correlations for Cretaceous paleoceanographic events worldwide. *EOS, Transactions of the American Geophysical Union* 82, 361–364.
- Kuhnt, W., Hess, S., Jian, Z., 1999. Quantitative composition of benthic foraminiferal assemblages as a proxy indicator for organic carbon flux rates in the South China Sea. *Marine Geology* 156, 123–127.
- Kuhnt, W., Luderer, F., Nederbragt, A., Thurow, J., Wagner, T., 2005. Orbital scale record of the late Cenomanian-Turonian Oceanic Anoxic Event (OAE 2) in the Tarfaya Basin (Morocco). *International Journal of Earth Sciences* 94, 147–159.
- Kuhnt, W., Nederbragt, A., Leine, L., 1997. Cyclicity of Cenomanian-Turonian organic-carbon-rich sediments in the Tarfaya Atlantic Coastal Basin (Morocco). *Cretaceous Research* 18, 587–601.
- Kuypers, M.M.M., Pancost, R.D., Nijenhuis, I.A., Sinninghe Damsté, J.S., 2002. Enhanced productivity led to increased organic carbon burial in the euxinic North Atlantic basin during the late Cenomanian oceanic anoxic event. *Paleoceanography* 17, 1051, doi:10.1029/2000PA000569.
- Larson, R.L., Erba, E., 1999. Onset of the mid-Cretaceous greenhouse in the Barremian-Aptian: iogenous event and the biological, sedimentary, and geochemical responses. *Paleoceanography* 14, 663–678.
- Lu, G., Adatte, T., Keller, G., Ortiz, N., 1998. Abrupt climatic, oceanographic and ecological changes near the Paleocene-Eocene transition in the deep Tethys basin: the Alademilla section, southern Spain. *Eclogae Geologicae Helveticae* 91, 293–306.
- Luderer, F., Kuhnt, W., 1997. A high resolution record of the Rotalipora extinction in laminated organic-rich limestones of the Tarfaya Atlantic coastal Basin (Morocco). *Annales de la Société Géologique Nord* 5, 199–205.
- Mackenzie, F.T., Lerman, A., Ver, L.M.B., 1998. Role of the continental margin in the global carbon balance during the past three centuries. *Geology* 26, 423–426.
- Mort, H.P., Adatte, T., Föllmi, K.B., Keller, G., Steinmann, P., Matera, V., Berner, Z., Stüben, D., 2007. Phosphorus and the roles of productivity and nutrient recycling during oceanic anoxic event 2. *Geology* 35, 483–486.
- Mort, H.P., Jaquat, O., Adatte, T., Steinmann, P., Föllmi, K., Matera, V., Berner, Z., Stüben, D., 2007a. The Cenomanian-Turonian anoxic event in Italy and Spain: enhanced productivity and/or better preservation. *Cretaceous Research* 28, 597–612.
- Mort, H.P., Jaquat, O., Adatte, T., Steinmann, P., Föllmi, K., Matera, V., Berner, Z., Stüben, D., 2007b. Phosphorus and the roles of productivity and nutrient recycling during Oceanic Anoxic Event 2. *Geology* 35, 483–486.
- Nederbragt, A.J., Thurow, J., Vonnhof, H., Brumsack, H.J., 2004. Modelling oceanic carbon and phosphorus fluxes: implications for the cause of the late

- Cenomanian Oceanic Anoxic Event (OAE 2). *Journal of the Geological Society, London* 141, 721–728.
- Paul, C.R.C., Lamolda, M.A., Mitchell, S.F., Vaziri, M.R., Gorostidi, A., Marshall, J.D., 1999. The Cenomanian-Turonian boundary at Eastbourne (Sussex, UK): a proposed European reference section. *Palaeogeography, Palaeoclimatology, Palaeoecology* 150, 83–121.
- Philip, J., 2003. Peri-Tethyan neritic carbonate areas: distribution through time and driving factors. *Palaeogeography, Palaeoclimatology, Palaeoecology* 196, 19–37.
- Racki, G., Cordey, F., 2000. Radiolarian palaeoecology and radiolarites: is the present the key to the past? *Earth-Science Reviews* 52, 83–120.
- Reicherter, K., Pletsch, T., Kuhnt, W., Manthey, J., Homeier, G., Wiedmann, J., Thurow, J., 1994. Mid-Cretaceous paleogeography and paleoceanography of the Betic Seaway (Betic Cordillera, Spain). *Palaeogeography, Palaeoclimatology, Palaeoecology* 107, 1–33.
- Rickaby, R.E.M., Elderfield, H., 1999. Planktonic foraminiferal Cd/Ca: paleonutrients or paleotemperature. *Paleoceanography* 14, 293–303.
- Rodríguez, J., Pascual, A., Elorza, J., 1998. Cenomanian events in the deep western Basque Basin: the Leioa section. *Cretaceous Research* 19, 673–700.
- Ruttenberg, K.C., 1992. Development of a sequential extraction method for different forms of phosphorus in marine sediments. *Limnology and Oceanography* 37, 1460–1482.
- Sahagian, D., Pinous, O., Olfieriev, A., Zakharov, V., Beisel, A., 1996. Eustatic curve for the middle Jurassic-Cretaceous based on Russian platform and Siberian stratigraphy: zonal resolution. *American Association of Petroleum Geologists* 80, 1433–1458.
- Schlanger, S.O., Jenkyns, H.C., 1976. Cretaceous oceanic anoxic events: causes and consequences. *Geologie en Mijnbouw* 55, 179–184.
- Schwenke, W., Kuhnt, W., 1992. Subsidence history and continental margin evolution of the Western Pyrenean and Basque Basins. *Palaeogeography, Palaeoclimatology, Palaeoecology* 95, 297–318.
- Sellwood, B.W., Price, G.P., Valdes, P.J., 1994. Cooler estimates for Cretaceous temperatures. *Nature* 370, 453–455.
- Singer, A., 1984. The palaeoclimate interpretation of clay minerals – a review. *Earth Science Reviews* 21, 251–293.
- Sinninghe Damsté, J.S., Koster, J., 1998. A euxinic southern North Atlantic Ocean during the Cenomanian/Turonian oceanic anoxic event. *Earth and Planetary Science Letters* 158, 165–173.
- Sinton, C.W., Duncan, R.A., 1997. Potential links between ocean plateau volcanism and global ocean anoxia at the Cenomanian-Turonian boundary. *Economic Geology and the Bulletin of the Society of Economic Geologists* 92, 836–842.
- Tamburini, F., Adatte, T., Föllmi, K., Bernasconi, S.M., Steinmann, P., 2003a. Investigating the history of East Asian monsoon and climate during the last glacial-interglacial period (0–140 000 years): mineralogy and geochemistry of ODP Sites 1143 and 1144, South China Sea. *Marine Geology* 201, 147–168.
- Tamburini, F., Föllmi, K., Adatte, T., 2003b. Sedimentary phosphorus record from the Oman margin: new evidence of high productivity during glacial periods. *Paleoceanography* 18, 1015, doi:10.1029/2000PA000616.
- Thompson, E.L., Schmitz, B., 1997. Barium and the late Paleocene  $\delta^{13}\text{C}$  maximum: evidence of increased marine surface productivity. *Paleoceanography* 12, 239–254.
- Tsikos, H., Jenkyns, H.C., Walsworth-Bell, B., Petrizzo, M.R., et al., 2004. Carbon-isotope stratigraphy recorded by the Cenomanian-Turonian Oceanic Anoxic Event: correlation and implications based on three key localities. *Journal of the Geological Society, London* 161, 711–719.
- Van Cappellen, P., Ingall, E.D., 1994. Benthic phosphorus regeneration, net primary production, and ocean anoxia – a model of the coupled marine biogeochemical cycles of carbon and phosphorus. *Paleoceanography* 9, 677–692.
- Van Cappellen, P., Ingall, E.D., 1996. Redox stabilization of the atmosphere and oceans by phosphorus-limited marine productivity. *Science* 271, 493–496.